TECHNISCHE UNIVERSITÄT WIEN

DIPLOMARBEIT

Investigation of Sputtering Properties of Tungsten Model Systems Relevant for Nuclear Fusion Devices

ausgeführt am
Institut für Angewandte Physik
der Technischen Universität Wien
Wiedner Hauptstraße 8-10 / E134
1040 Wien

unter der Anleitung von
Univ.Prof. Dr.techn. Friedrich Aumayr

und
Dipl.-Ing. Christian Cupak, BSc

durch
Martina Fellinger, BSc
fellinger@iap.tuwien.ac.at
Matrikelnummer: 01620771
[redacted]

Wien, März 2022 Martina Fellinger, BSc.

Die approbierte gedruckte Originalversion dieser Diplomarbeit ist an der TU Wien Bibliothek verfügbar
The approved original version of this thesis is available in print at TU Wien Bibliothek.

Die approbierte gedruckte Originalversion dieser Diplomarbeit ist an der TU Wien Bibliothek verfügbar
The approved original version of this thesis is available in print at TU Wien Bibliothek.

Kurzfassung

Die Entwicklung einer Möglichkeit die immense nukleare Energie von Fusionsprozessen technisch nutzbar zu machen ist ein ambitioniertes Unterfangen, dessen Umsetzung seit Jahr- zehnten von Wissenschaft und Technik angestrebt wird. Zukünftige Reaktoren werden stetig geplant und weiterentwickelt. Neueste Erkenntnisse bei der Entwicklung und Testung möglicher Operationsmodi haben gezeigt, dass die Wissenschaft mit heutigen Mitteln so nah an der technischen Realisierung der Kernfusionsenergie als sichere, effiziente und kohlenstoffarme Energiequelle steht wie noch nie.
Allerdings gibt es vor dem tatsächlichen Bau eines konventionell nutzbaren Fusionsreaktors noch Aspekte, die weitere wissenschaftliche Untersuchungen benötigen. Ein bisher noch nicht vollständig untersuchtes Gebiet beschäftigt sich mit dem Verhalten von Wandmaterialen, mit denen die Innenseiten des Reaktors ausgekleidet werden. Sowohl Erosions- als auch Implantationsprozesse werden in zukünftigen Reaktoren dynamisch auftreten. Die Eigenschaften der verwendeten Stoffe müssen dabei kritischen Auswahlkriterien für potentielle Wandmaterialien genügen, da ins Plasma erodierte Teilchen die Effektivität des Reaktors stark drosseln.

Aus diesem Grund wurde im Zuge dieser Diplomarbeit das Zerstäubungsverhalten von reinen Wolfram (W) Schichten sowie von re-deponierten W Schichten untersucht. Dazu wurden zwei präzise Quarz-Kristall-Mikrowaagen (QCM) gemeinsam mit einem zweckoptimierten Aufbau am IAP TU Wien verwendet. Das experimentelle Setup wurde im Zuge dieser Arbeit erweitert und mit Motoren bestückt, sodass nun vollautomatische Messprozedere durchgeführt werden können. Zusätzlich zur experimentellen Arbeit wurden ergänzende Simulationen durchgeführt, um einen Vergleich mit den Messdaten zu ermöglichen.
Ergebnisse haben gezeigt, dass die Absolutwerte der Zerstäubungsausbeuten für die verwendeten Schichten aus reinem W sowie re-deponiertem W vergleichbar sind. Eine detaillierte Analyse der Abhängigkeit der Zerstäubungsausbeute vom Ioneneinfallswinkel lässt außerdem auf interessante physikalische Konsequenzen, nämlich mögliche Kristallstrukturen auf einer den verwendeten Proben, schließen.

Die Resultate aus dieser Arbeit tragen zum Fortschritt des europäischen Konsortiums für die Entwicklung von Fusionsenergie, EUROFusion, im Zuge des Projekts ”Plasma-Wall Interaction & Exhaust (PWIE) - Subproject SP B” bei.

Die approbierte gedruckte Originalversion dieser Diplomarbeit ist an der TU Wien Bibliothek verfügbar
The approved original version of this thesis is available in print at TU Wien Bibliothek.
TU Bibliothek Your knowledge hub WIEN

Abstract

An implementation utilising the huge amounts of nuclear energy released in the process of fusing light nuclei to heavier ones is an ambitious project, whose realisation has by now been pursued by science and technology over several decades. Future fusion reactors are presently being planned and recent results obtained at test beds for such devices revealed promising data, suggesting that fusion as a safe, efficient and low-carbon energy supply is on its way to make expectations meet.
However, various issues concerning this proposal still need profound analyses. One aspect that is tackled in the course of this project, are properties of potential first wall materials directly facing the plasma in fusion devices. Erosion as well as implantation processes will occur dynamically due to plasma wall interactions inside the reactor. Hence, sputtering behaviours of relevant wall coating materials and additionally redeposited layers thereof are of great interest for fusion research. This concern arises from the fact that properties like erosion form crucial selection criteria for first wall coatings, since eroded particles drastically reduce the reactor efficiency.

In this work, a precise twofold quartz crystal microbalance (QCM) measurement technique combined with a dedicated sputtering setup at IAP TU Wien was successfully employed in order to measure sputtering properties of pure tungsten (W) as well as redeposited W layers. The experimental setup has been upgraded in the course of this thesis, enabling to perform sophisticated measurement routines entirely remotely. Additionally, numerical simulations were performed for comparison.
Results have shown that the absolute values of sputter yields as well as the angular distribution of sputtered particles show comparable values for both the pure W target and the sample hosting an additional layer containing redeposited W. However, a more detailed look onto the dependence of the sputter yields on ion incidence angles has revealed interesting physical behaviour, suggesting specific crystal structures on one of the utilised samples.

The outcome of this project contributed to the scientific progress in the work package ”Plasma Wall Interaction & Exhaust (PWIE) - Subproject SP B” of the European consortium for the development of fusion energy, EUROfusion.

Die approbierte gedruckte Originalversion dieser Diplomarbeit ist an der TU Wien Bibliothek verfügbar
The approved original version of this thesis is available in print at TU Wien Bibliothek.
TU Bibliothek Your knowledge hub WIEN

List of scientific contributions

Publications in scientific journals

C. Cupak, P. S. Szabo, H. Biber, R. Stadlmayr, C. Grave, M. Fellinger, J. Brötzner, R. A. Wilhelm, W. Möller, A. Mutzke, M. V. Moro, F. Aumayr. Sputter yields of rough surfaces: Importance of the mean surface inclination angle from nano- to microscopic rough regimes. *Applied Surface Science* **570** (2021) [1].

C. Watzenböck, M. Fellinger, K. Held, A. Toschi. Long-term memory magnetic correlations in the Hubbard model: A dynamical mean-field theory analysis. (submitted, 2022) [2].

A. Lopez-Cazalilla, C. Cupak, M. Fellinger, F. Granberg, P. S. Szabo, A. Mutzke, K. Nordlund, F. Aumayr, R. Gonzalez-Arrabal. Comparative study regarding the sputtering yield of nano-columnar tungsten surfaces under Ar^+ irradiation. (submitted, 2022) [3].

Research stays

Uppsala Universitet, Department of Physics and Astronomy, Prof. Daniel Primetzhofer. Experimental campaigns: *In-situ* measurement of implanted D concentrations in Be bulk samples via ERDA and simultaneous TDS investigation; Installation of a QCM setup to study YH_2 growth rates and subsequent oxidation processes *in-situ*.
Uppsala (Sweden), 16.10.2021 - 31.10.2021

Talks and Poster Presentations

M. Fellinger. Sputtering of redeposited tungsten layers. Midterm monitoring meeting of the EUROfusion Work Package ”Plasma Wall Interaction & Exhaust (PWIE)” - Subproject SP B: ”Experiments on erosion, deposition and material migration”.
Online Meeting, 13.10.2021

M. Fellinger, C. Cupak, H. Biber, E. Pitthan, M. V. Moro, K. Hradil, D. Primetzhofer, F. Aumayr. ”Investigation of Sputtering Properties of Tungsten Model Systems Relevant for Nuclear Fusion Devices”.
Franz Viehböck poster competition - Silver Medal Winner, 29.11.2021

C. Cupak, M. Fellinger, H. Biber, A. Redl, A. Lopez-Cazalilla, R. Gonzalez-Arrabal, F. Aumayr. ”Sputtering of highly corrugated, nano-columnar W surfaces: An option for the first wall coating of nuclear fusion devices?”.
Symposium on Surface Science 2022 (3S*22), 16.3.2022

Die approbierte gedruckte Originalversion dieser Diplomarbeit ist an der TU Wien Bibliothek verfügbar
The approved original version of this thesis is available in print at TU Wien Bibliothek.
TU Bibliothek Your knowledge hub WIEN

Contents

Die approbierte gedruckte Originalversion dieser Diplomarbeit ist an der TU Wien Bibliothek verfügbar
The approved original version of this thesis is available in print at TU Wien Bibliothek.
TU Bibliothek Your knowledge hub WIEN

Die approbierte gedruckte Originalversion dieser Diplomarbeit ist an der TU Wien Bibliothek verfügbar
The approved original version of this thesis is available in print at TU Wien Bibliothek.

1. Introduction

Finding a sustainable, clean and highly efficient energy source has hardly been more important that in times of climate changes. An elegant idea that arose on the way seeking for energy resources generally, is to learn a lesson from our sun and mimic its nature of generating power by merging light nuclei to heavier ones. However, releasing feasible net energy out of such fusion processes is an ambitious idea, whose implementation has already been pursued over several decades. Various methods have been discussed over times, some of them with more success than others. Nevertheless, one of the most promising concepts that is on its way to make expectations meet is the Tokamak reactor concept [4, 5].

Despite limitations on commercially disposing fusion as energy source, recent developments at the Joint European Torus (JET) accomplished by researchers from EUROfusion, the European consortium for the development of fusion energy, have revealed promising data. At JET, record-breaking 59 MJ of fusion energy were produced via a deuterium-tritium fuel plasma. Such and other milestones that have been accomplished in the last years cast positive light on the evolution of fusion as a safe, efficient and low-carbon energy supply. The latest results are fully in line with predictions for ITER, which is a fusion reactor, currently under construction, that will be the first fusion device to produce net energy [6–8].

1.1. Fusion process and Tokamak reactor concept

The Tokomak reactor is designed to host controlled fusion processes inside a torus-shaped reactor vessel. The desired fusion process at JET and ITER, where a tritium and a deuterium nucleus merge to a high-energetic helium nucleus via additionally releasing a kinetic neutron, is depicted in figure 1.1 [9].

Die approbierte gedruckte Originalversion dieser Diplomarbeit ist an der TU Wien Bibliothek verfügbar
The approved original version of this thesis is available in print at TU Wien Bibliothek.
TU Bibliothek Your knowledge hub WIEN

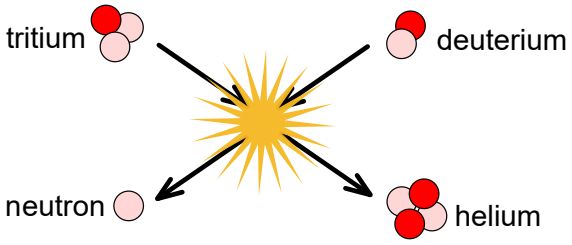

Figure 1.1.: Sketch of a deuterium-tritium fusion process.

In order to make such reactions feasible, the fusion plasma inside the toroidal reactor core must be held at an approximate temperature of $1.5 \cdot 10^8$ K. A dedicated arrangement of field coils generate toroidal and vertical magnetic fields penetrating the reactor vessel. This results in a superposition with an additional poloidal magnetic field, generated by a torodial plasma current, driven by the reactor's central solenoid. The resulting helically shaped magnetic field ensures that the plasma ions are trapped inside the torus. However, such a magnetic confinement of high-energetic ions demands sophisticated techniques and forms an ongoing field of research [10].

Another important aspect that still requires investigation is the reactor vessel's first inner wall. The reactor parts closest to the plasma, so called plasma facing components, are covered with first wall materials, that are designed to withstand the harsh physical conditions present in the reactor. Especially at the divertor region, which is located at the bottom of the torus, where the last closed magnetic field lines are ending (see figure 1.2), high requirements on the wall coatings are demanded, as the divertor enables fuel and heat exchange [11].

Despite the magnetic confinement, some plasma ions will, however, interact with the vessel wall. Any erosion processes occurring might lead to impurities in the plasma and will in any case limit the reactor's efficiency. Such events therefore need to be studied and investigated beforehand as detailed as possible [12, 13].

Die approbierte gedruckte Originalversion dieser Diplomarbeit ist an der TU Wien Bibliothek verfügbar
The approved original version of this thesis is available in print at TU Wien Bibliothek.

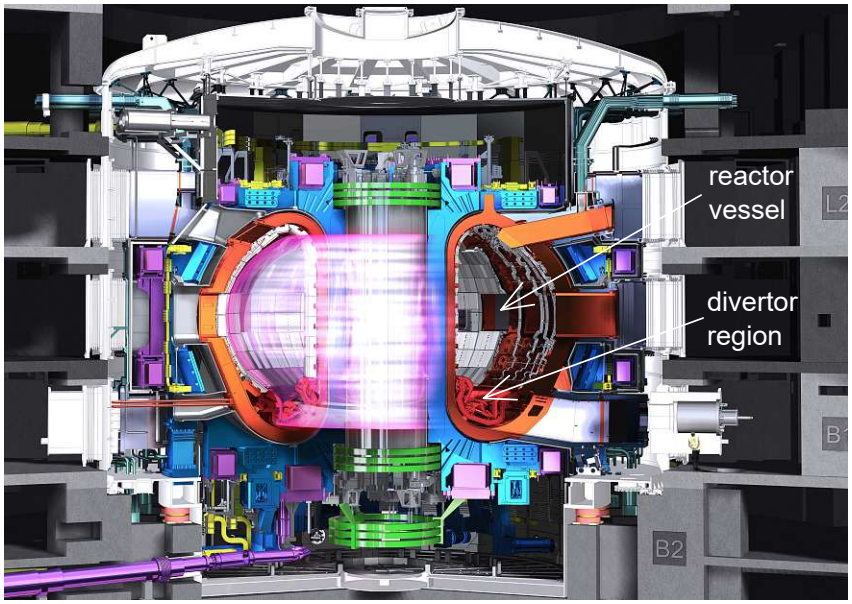

Figure 1.2.: Cross section of a Tokamak reactor. Picture taken from [6].

1.2. Motivation

One way to study erosion processes of potential first wall materials is to make use of a highly precise measurement technique, the quartz crystal microbalance (QCM). This technique enables to measure tiny mass changes at orders of 10^{-9} g/s (see e.g. [14]) *in-situ* and therefore allows to study erosion and implantation processes in great detail. Both erosion and implantation will occur in a future fusion reactor dynamically alongside each other, and it might additionally happen that sputtered material can be redeposited on different wall parts. Such redepositions for their part again happen simultaneously to implantation processes. Due to the instantaneous incorporation of fuel species during the redeposition, erosion properties of these generated layers might differ from original material characteristics. This motivates to investigate sputtering properties of relevant systems in general as well as to study sputtering of redeposited layers consisting of potential first wall materials [15].

In the next section of this document the theoretical aspects laying behind the QCM measurement technique are discussed. Chapter 3 explains the basics of the experimental setup and illustrates upgrades that were performed in the course of this project. Finally, obtained results are illustrated and discussed in chapter 4 before a potential outlook and a conclusion are given in chapter 5.

Die approbierte gedruckte Originalversion dieser Diplomarbeit ist an der TU Wien Bibliothek verfügbar
The approved original version of this thesis is available in print at TU Wien Bibliothek.
TU Bibliothek Your knowledge hub WIEN

2. Theoretical background

2.1. Quartz crystal microbalance (QCM) measurement technique

The QCM measurement technique is a useful method to determine mass change rates in real time inside a vacuum chamber. Due to its high sensitivity, mass change rates down to 10^{-9} g/s can be detected [14].

The underlying principle of any QCM can be described by the well-known Sauerbrey equation that combines mass changes and eigenfrequency changes of a given quartz crystal [16]

$$\frac{\Delta m}{m_Q} = -\frac{\Delta f}{f_Q}, \tag{2.1}$$

where Δm and m_Q denote absolute mass changes and inital quartz mass, Δf and f_Q are the absolute eigenfrequency change and the quartz' inital resonance frequency, respectively.

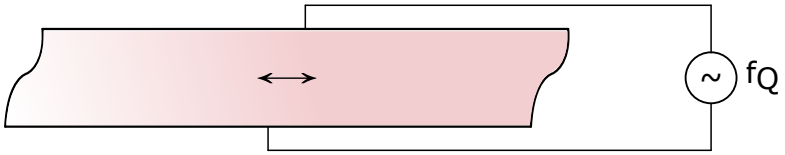

Figure 2.1.: Sketch of a shear mode thickness oscillation of a quartz crystal generated by an applied alternating electric field.

More precisely, a quartz crystal can be excited to perform a shear-mode thickness oscillation at its resonance frequency, schematically depicted in figure 2.1. The excitation can be applied electronically by making use of the piezoelectric effect via applying an alternating current onto the quartz. The resulting oscillating circuit has a specified eigenfrequency, whose relative changes $\Delta f/f_Q$ are then proportional to the relative mass changes of the quartz $-\Delta m/m_Q$ enabling to detect mass changes by measuring temporal frequency changes [17, 18].

In addition, one can apply layers of any material of interest on top of a quartz crystal to investigate its erosion and implantation under ion bombardment. Nevertheless, in order not to violate equation (2.1) the coating layer needs to be sufficiently thin in comparison to the total thickness of the quartz [17]. A general rule of thumb, established at IAP TU

Die approbierte gedruckte Originalversion dieser Diplomarbeit ist an der TU Wien Bibliothek verfügbar
The approved original version of this thesis is available in print at TU Wien Bibliothek.

Wien suggests not to exceed 300 nm of W on top of a resonator disk. Additionaly, it is important to mention that the mass changes ought to arise at an area, where the quartz is sufficiently sensitive. In essence, the quartz' sensitivity curve resembles a Gaussian function having its peak in the quartz centre and decreasing radially outwards from the centre. This is especially important for setups, where mass changes of the quartz are induced by ion bombardment. For such sputtering processes, it is therefore important to ensure a homogeneous irradiation throughout the whole sensitive area of the quartz [19, 20].

2.2. Sputter yield calculation

2.2.1. Erosion rates - QCM target approach

Regarding ion beam erosion experiments it is convenient to quantify the relative erosion in terms of sputter yields y_t, defined as mass changes per impinging ion

$$y_T \left[\frac{amu}{ion}\right] = -\frac{\Delta m_{amu}}{N_{ions}}, \tag{2.2}$$

where Δm_{amu} stands for the mass change in atomic mass units per cm^2 and N_{ions} denotes the number of impinging ions per cm^2. As the conversion from atomic mass units to SI-units reads

$$\Delta m_{amu} = \frac{\Delta m}{A_Q \cdot m_0}, \tag{2.3}$$

with Δm representing the absolute mass changes in kg, A_Q being the area in cm^2 and $m_0 = 1.66 \cdot 10^{-27}$ kg/amu being the atomic mass unit and additionally

$$m_Q = A_Q \cdot d_Q \cdot \rho_Q, \tag{2.4}$$

where d_Q and ρ_Q denote thickness and density of the quartz, respectively, the atomic mass change can be rewritten to find

$$\Delta m_{amu} = -\frac{\Delta f \cdot m_Q}{A_Q \cdot m_0 \cdot f_Q} = -\frac{\Delta f \cdot d_Q \cdot \rho_Q}{m_0 \cdot f_Q}. \tag{2.5}$$

It should be stressed that, additionally, the Sauerbrey equation (2.1) was exploited in the last step, which allows to calculate the atomic mass change by means of QCM frequency recording. Furthermore, by assuming a known ion current density j, which is approximately constant throughout the experimental time duration Δt, the number of impinging ions per cm^2 can be formulated as

$$N_{ions} = \frac{j \cdot \Delta t}{q \cdot e_0}, \tag{2.6}$$

Die approbierte gedruckte Originalversion dieser Diplomarbeit ist an der TU Wien Bibliothek verfügbar
The approved original version of this thesis is available in print at TU Wien Bibliothek.

where q and e_0 denote ion charge state and elementary charge, respectively. Inserting equations (2.5) and (2.6) into (2.2) results in

$$y_T \left[\frac{amu}{ion}\right] = -\frac{\Delta m_{amu}}{N_{ions}} = \frac{\Delta f}{\Delta t} \cdot \frac{1}{j} \cdot \frac{q \cdot e_0 \cdot d_Q \cdot \rho_Q}{m_0 \cdot f_Q}. \tag{2.7}$$

Ultimately, by assuming a pure target composition, where m_T is the atomic mass of the relevant element, the final expression for the sputter yield Y_t in terms of released atoms per impinging ions is achieved

$$Y_T \left[\frac{atoms}{ion}\right] = \frac{eroded\ particles}{impinging\ ions} = \frac{y_T}{m_T} = \frac{\Delta f}{\Delta t} \cdot \frac{1}{j} \cdot \frac{q \cdot e_0 \cdot d_Q \cdot \rho_Q}{m_0 \cdot f_Q \cdot m_T}. \tag{2.8}$$

Equation (2.8) therefore describes the erosion rate of a desired target material of interest exposed to bombardment with ions of well-defined charge state q and piecewise constant current j [17, 18, 21–23].

2.2.2. Deposition rates - QCM catcher approach

As not only the net mass difference of material layers under ion bombardment are of interest for the investigation of sputtering, but also the behaviour of the released particles from the target surface constitutes an interesting property, a secondary QCM that catches the sputtered particles from the primary target can be used [24]. This enables additionally probing, e.g., the angular distribution of the released atoms. A sketch of the arrangement of the twofold QCM technique is visualised in figure 2.2.

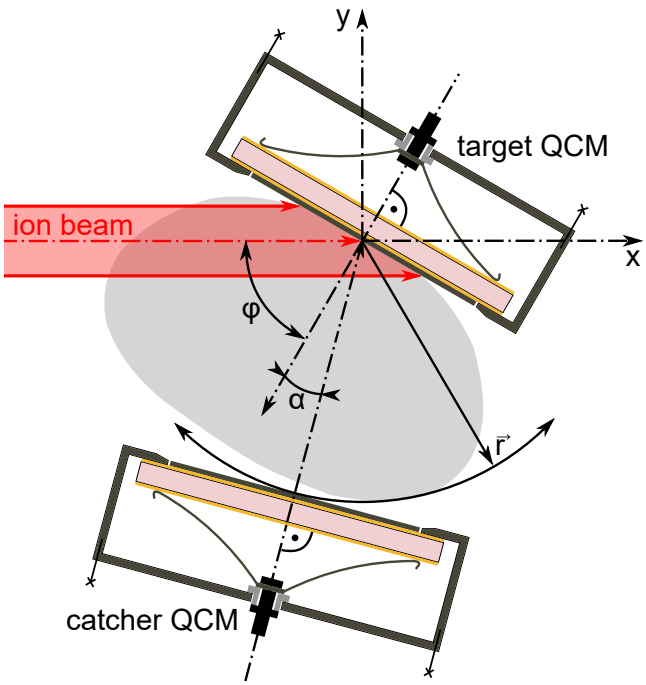

Figure 2.2.: Sketch of the QCM setup used to detect mass differences, adapted from [25].

Die approbierte gedruckte Originalversion dieser Diplomarbeit ist an der TU Wien Bibliothek verfügbar
The approved original version of this thesis is available in print at TU Wien Bibliothek.

The quantification of mass changes due to deposited particles at the catcher QCM then functions analogously to the formulation of a sputter yield for erosion processes, given in (2.8). However, in this configuration there is no longer a well-defined and shaped incoming particle flux present, impinging on the catcher surface. There is rather a distribution of diverging trajectories for the sputtered atoms originating from a releasing point at the target surface approaching the catcher surface. Nevertheless, the primary ions hitting the target still resemble a well shaped beam and the current density j in equation (2.6) can now be expressed via the total current I

$$N_{ions} = \frac{I \cdot \Delta t}{q \cdot e_0} = \frac{j \cdot A_Q \cdot \Delta t}{q \cdot e_0}, \tag{2.9}$$

where A_Q again denotes the scanning area at the target, whereon the ions land. In the same manner as for erosion processes, the mass differences occurring on the catcher QCM via deposition processes can be written as

$$\Delta m_{amu} = -\frac{\Delta f \cdot d_Q \cdot \rho_Q}{m_0 \cdot f_Q}. \tag{2.10}$$

In full analogy to target sputter yields, these expressions are now combined to result in the catcher yield Y_C in terms of deposited particles per impinging ion

$$Y_C \left[\frac{atoms}{ion}\right] = \frac{deposited\ particles}{impinging\ ions} = \frac{y_C}{m_C} = -\frac{\Delta f}{\Delta t} \cdot \frac{1}{I} \cdot \frac{q \cdot e_0 \cdot d_Q \cdot \rho_Q}{m_0 \cdot f_Q \cdot m_C}, \tag{2.11}$$

where m_C denotes the atomic mass of the catcher material. Concerning the latter, it is conventional, at least in our setup, to use the same type of material for both target and catcher coatings. This supports the assumption of an ideal sticking probability of 100% on the catcher quartz resulting in a direct deposition of every incoming particle [25, 26].

Besides this approximation, in the derivation of equation (2.11) it is furthermore ignored that reflected ions from the target may as well induce sputtering processes at the catcher surface. The detected catcher frequency signal therefore rather results from a combination of deposition and erosion processes. However, as the contribution from reflected ions makes up only a marginal part, at least for the geometries utililsed in our experiments, equation (2.11) usually forms a sufficiently accurate formulation for most practical purposes and compares well with simulation results [1].

As already stated before, for the applicability of equation (2.1) it is important to ensure a homogeneous particle bombardment over a sufficiently large area on the quartz. However, concerning the released particles from the target surface approaching the catcher we have no bearing on their trajectories. The catcher yield Y_C should therefore be interpreted as a measure to probe the distribution of sputtered particles, mathematically resembling a convolution of the quartz' sensitivity function and the angular distribution of the incoming particles.

Die approbierte gedruckte Originalversion dieser Diplomarbeit ist an der TU Wien Bibliothek verfügbar
The approved original version of this thesis is available in print at TU Wien Bibliothek.

It should be noted at this point that the sign in equation (2.11) is different from the one in (2.8). The sign convention is conveniently chosen to identify positive catcher yields with mass increases.

More rigorous details on the QCM measurement technique can be found in the outlined literature [17, 18, 20, 24].

2.3. Dual mode temperature compensation

While the Sauerbrey equation (2.1) is a fundamental relation that combines mass and eigenfrequency of a quartz crystal, mass changes are not the only quantity affecting a quartz' oscillation. Particularly, when mass changes during a measurement are comparably small, other dynamic state variables can influence the frequency signal severely.

Precisely, besides mass changes also temperature changes induce eigenfrequency drifts on a quartz. Hence, experiments to detect mass changes can hardly be performed during severe temperature modifications, as it is, e.g., the case when performing temperature programmed desorption measurements. Also, effects induced by small temperature fluctuations, which might naturally occur inside laboratories, can sometimes outweigh signals originating from real mass changes, as it is the case when measuring small sputter yields, as, e.g., for D_2^+ irradiation of W.

Though fortunately, every quartz crystal is also its own temperature sensor. I want to stress that equation (2.1) is not restricted to a single frequency mode. Besides the commonly used fundamental shear-mode thickness oscillation f_1, schematically depicted in figure 2.1, one can also drive the quartz crystal in its third overtone mode f_3. The combination of these two allows to derive a beat frequency

$$f_b = 3 \cdot f_1 - f_3. \tag{2.12}$$

This quantity turns out to show a nearly linear dependence on temperature [27].

Hence, by exciting both modes quasi-simultaneously the beat frequency can be used as a quartz intrinsic parameter and both modes can be expressed in terms of f_b. This finally enables to compensate all temperature effects out of the detected frequency signals to ultimately arrive at purely mass dependent data.

More mathematical details lying behind this measurement technique can be found in reference [14]. Possibilities and limitations of this dual mode procedure were studied in a previous project, whereas details can be found in reference [28].

Die approbierte gedruckte Originalversion dieser Diplomarbeit ist an der TU Wien Bibliothek verfügbar
The approved original version of this thesis is available in print at TU Wien Bibliothek.
TU Bibliothek Your knowledge hub WIEN

2.4. Simulation Methods

Since a comparison of the experimentally obtained data to numerically calculated values is given in chapter 4 of this document, the principles behind the exploited simulation routine, utilised in the course of this project, are briefly mentioned in this section.

Many modern techniques designed to simulate sputtering processes base on the binary collision approximation, where the impinging ion on a surface is approximated to travel through a material by undergoing binary elastic collisions with target atoms that are fully independent from each other [29, 30]. Between these assumed elastic collisions, the ion loses kinetic energy via electronic stopping [31]. The simulation code employed during this project, SDTrimSP, is a tool developed at the Max Planck Institute for Plasma Physics [32]. It is constructed to simulate ion surface interaction under defined conditions, as, e.g., for given ion incidence angles, ion energy, target composition, etc., and calculates collision cascades of ions that are shot onto amorphous solids by means of Monte Carlo methods.

Precisely, I utilised a recently developed graphical user interface for SDTrimSP simulations in order to conduct the calculations [33]. More details on the simulation method can be found in the outlined literature [29–32].

Die approbierte gedruckte Originalversion dieser Diplomarbeit ist an der TU Wien Bibliothek verfügbar
The approved original version of this thesis is available in print at TU Wien Bibliothek.

3. Experimental methods

3.1. Overview of the experimental setup

Sputter yield measurements demand various constraints on the environmental conditions present during the experiment. On these grounds, a dedicated sputter investigation setup located in the Augustin laboratory at IAP TU Wien was utilised. This arrangement consists of a vacuum chamber equipped with several devices and instruments, which are shortly illustrated in the following.

In order to keep contaminations on the samples of interest on a minimum, the experimental chamber is constantly evacuated via a pre-vacuum rotary vane pump and additional three turbomolecular pumps. Thereby, base pressure values of approximately $1.0 \cdot 10^{-9}$ mbar can be reached in idle conditions.
The experimental setup, depicted schematically in figure 3.1, hosts an apparatus containing the twofold QCM setup inside the central vacuum chamber. A more detailed sketch of the QCM target and catcher setup has already been shown in figure 2.2 in the previous chapter. Both target and catcher QCM are mounted in the chamber via manipulators to allow for position changes of the samples. The samples can then be arranged in such a way that an ion beam can hit its surface. However, in order to properly create and accurately focus an ion beam onto a surface, this ion beam needs to be generated by peripheral devices.
Firstly, a desired ion species has to be created. For this purpose, a SPECS IQE 12/38 ion source was used, which can be supplied with defined amounts of working gas with desired composition. As visualised in figure 3.1, the working gas, e.g. Ar or D_2, can be mixed inside a mixing volume before getting forwarded to the ion gun via a thermovalve (TV). The TV enables pressure controlling of the working gas, i.e. a specific pressure inside the gun, that will later turn out to be proportional to the amount of ions reaching the sample. The latter can be defined and tuned via partially opening or closing the preceding valve thermally.
Inside the gun, the working gas gets ionised via electron collisions. The electrons are emitted from a tungsten cathode that is heated and supplied with a bias voltage. An applied acceleration voltage then extracts the positively charged ions out of the ionisation volume towards the beam shaping sections in the experiment.

Die approbierte gedruckte Originalversion dieser Diplomarbeit ist an der TU Wien Bibliothek verfügbar
The approved original version of this thesis is available in print at TU Wien Bibliothek.
TU Bibliothek Your knowledge hub WIEN

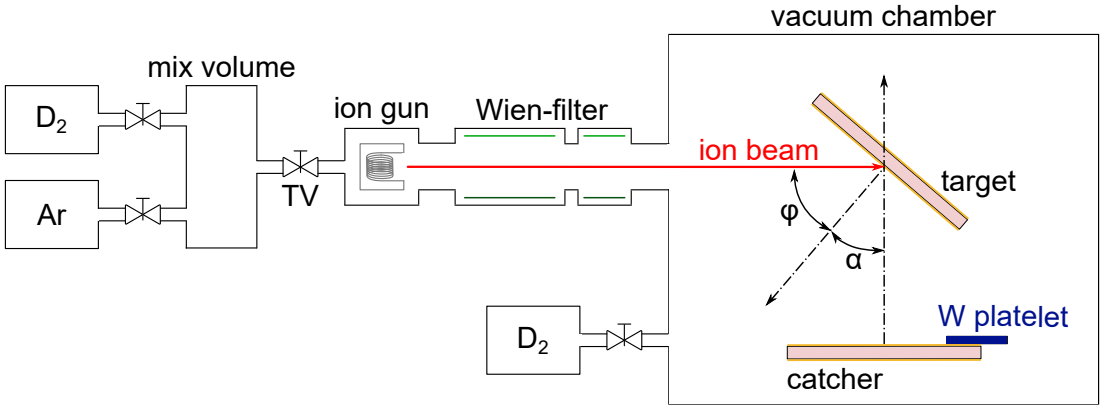

Figure 3.1.: Sketch of the overall experimental setup inlcuding: D_2 and Ar gas inlets; a mixing volume to properly mix desired gas species; a thermovalve (TV) for pressure controlling of the working gas; an ion gun to ionise the working gas; a Wien-filter for particle selection; a vacuum chamber hosting a twofold QCM apparatus and a W platelet; an additional D_2 gas inlet to the main vacuum chamber.

After the ion gun, a Wien-filter is assembled. Via a constant magnetic field, which is applied by a permanent magnet, and a certain electric field, established by a chosen deflection voltage on two capacitor plates, this section ensures that only ion types of a specific charge over mass ratio manage to approach the final chamber. Unwanted charge states as well as impurities get deflected by the magnetic field. Neutral components that are not affected by neither the electric nor the magnetic field are also sorted out by the geometry of the filter, which introduces a certain tilt of 1.2° for the transmission direction respective the input beam axis.
Subsequently, beam shaping instruments, i.e. electronic lenses and deflection plates, ensure that the beam can be focussed and scanned in order to provide a quasi homogeneous sample irradiation as this is crucial for the QCM performance. Having passed these sections, the generated ions can then finally enter the experimental chamber hosting the QCM arrangement. The ion shaping parameters specifically utilised in the course of this project are outlined in appendix A.
In order to determine the ion current density hitting the QCM, as this is important for a proper calculation of sputter yields given in (2.8) in the previous chapter, a Farady cup (FC) located on the QCM sample holder can be exploited. Via manipulator movements one can drive either the sample itself or the FC into the beam enabling to measure beam profiles of the utilised ion scannings. It should be stressed that as the ion current density is not perfectly constant throughout experiments, certain errors are picked up. In order to get a quantitative image of the error induced by beam fluctuations, it is useful to detect beam profiles various times during the measurement procudere, e.g. at the beginning and the end of the experiment. The difference between the detected profiles can then be used as basis for error calculations concerning the sputter yield. A detailed view on experimental routines also containing beam profile measurements is given in sections 3.2.2 and 3.2.3.
Control panels and power supplies of most setup components are positioned inside a

Die approbierte gedruckte Originalversion dieser Diplomarbeit ist an der TU Wien Bibliothek verfügbar
The approved original version of this thesis is available in print at TU Wien Bibliothek.
TU Bibliothek Your knowledge hub WIEN

rack next to the vacuum chamber. Next to digital data transfer via USB or GPIB interfaces, also analog output signals are forwarded via A/D converters towards a computer, allowing control of the experiment [25].

While the theoretical concepts of a QCM have already been outlined in the previous chapter, more focus is now laid on the experimental details using a quartz as a measurement tool. The quartz crystal itself is cut in a specifically chosen SC-cutting angle, manufactured by KVG Quartz Crystal Technology GmbH, Germany. The disk is furthermore coated on both sides with approximately 140 nm thin Au layers that function as electrical contacts. From these contacts, a central QCM wire and an earth lead are led out of the chamber via a feedthrough. Additionally, a not contacted dummy wire, which is designed to compensate for the cables' electrical resistivity, is assembled. Due to the high-frequency nature of the signals conducted through these cables, all components in the circuit need to be coaxial cables and the corresponding shieldings need to be incorporated as well. Ultimaltely, this makes up a total of four pins, i.e. earth lead, dummy wire, central quartz wire and the quartz wire's shiedling, that are led out of the chamber via feedthroughs.
It furthermore turns out that by exciting the crystal to perform an oscillation, the total circuit shows an impedance minimum at the quartz' resonance frequency. This effect can be exploited to generate a representative V_c voltage, which can be achieved via a so-called phase box containing dedicated electronics, developed and ugraded during years at IAP. The V_c analogue output can vary within a range of ± 10 V and is exactly zero, if the quartz oscillates in resonance. Forwarding this value via A/D converters to a computer enables to keep track of the resonance frequency by regulating a frequency generator using the V_c voltage as input variable for a virtual proportional-integral-derivative controller. The precise frequency of the sine wave for the quartz excitation, applied via a Tektronix AFG31000 function generator, that corresponds to an approximately zero V_c value, can be stored as momentary eigenfrequency in a list file for posteriori data evaluation. More details on the electronic circuitry and technical functionality of the phase box electronics can be found in reference [18], while elaborations on the controlling technique are illustrated in reference [34].

As already mentioned in the theory section, this controlling circuit is not limited to specific excitation modes, but can be extended towards excitations of two different modes quasi-simultaneously, the ground and third overtone mode. Hence, this enables to compensate potential temperature effects in the post-processing of the data. Reports on dual mode controlling techniques and the advantages as well as intricacies of this method are outlined in reference [14, 28].

Die approbierte gedruckte Originalversion dieser Diplomarbeit ist an der TU Wien Bibliothek verfügbar
The approved original version of this thesis is available in print at TU Wien Bibliothek.
TU Bibliothek Your knowledge hub WIEN

3.2. Setup upgrades

3.2.1. Manipulator motorization

As stated before, the samples of interest can be positioned inside the vacuum chamber via manipulators that allow for movements of both catcher and target quartz. While the most crucial axes of the target manipulator, allowing for movement in the z- and y-direction as well as rotating around the z-axis, had already been equipped with motors before starting this project, several other movement axes still required manual adjustments. However, measurements requiring very precise and recurring catcher movements turned out to gain importance when studying sputtering properties. Motorising the corresponding manipulator parts would therefore simplify the experimental procedures and enable performing measurements remotely without time constraints. Hence, the advantages of a fully automated experimental setup were clear, which is why a completion of the manipulator motorisation was performed in the course of this project.

Technical construction

Firstly, before motorising the remaining movable parts, an adapter construction for the manipulators, where the motors could be supported, was needed. Figure 3.2 shows the state of the art prior the upgrade. The respective manipulator axes that needed motorization, corresponding to the x-direction of the target QCM, x- and y-direction of the catcher QCM, as well as the y-axis rotation for the latter, are sketched in figure 3.2. Because of the excentrical and tilted orientation of the manipulator axis used to rotate the catcher QCM around the y-direction (see (1) in figure 3.2) and due to structural restrictions that prohibited to precisely measure the tilt angle of this manipulator element, a rather flexible design for the motor support was needed. CAD drawings of the designed construction are shown in figure 3.3. The left-hand side of figure 3.3 shows the catcher manipulator containing three motors for the manipulator axes 1,2 and 3, depicted also in figure 3.2. The right-hand side shows the construction for motor 4 corresponding to the target manipulator x-direction.

Die approbierte gedruckte Originalversion dieser Diplomarbeit ist an der TU Wien Bibliothek verfügbar
The approved original version of this thesis is available in print at TU Wien Bibliothek.

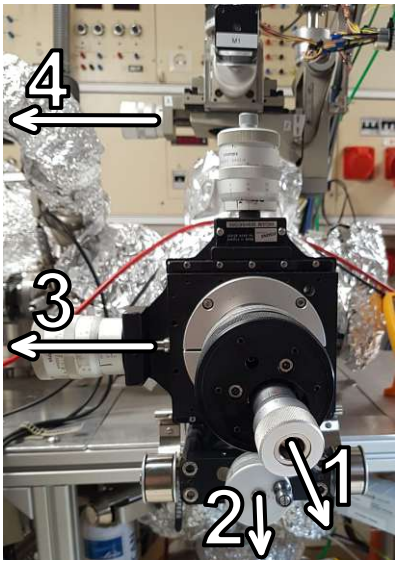

Figure 3.2.: Photo of the manipulators prior applying constructional elements. Axis 1 enables rotation of the catcher QCM around the x axis. Axis 2 corresponds to the catcher y-direction. Axis 3 corresponds to the catcher x direction and axis 4 corresponds to the target x direction.

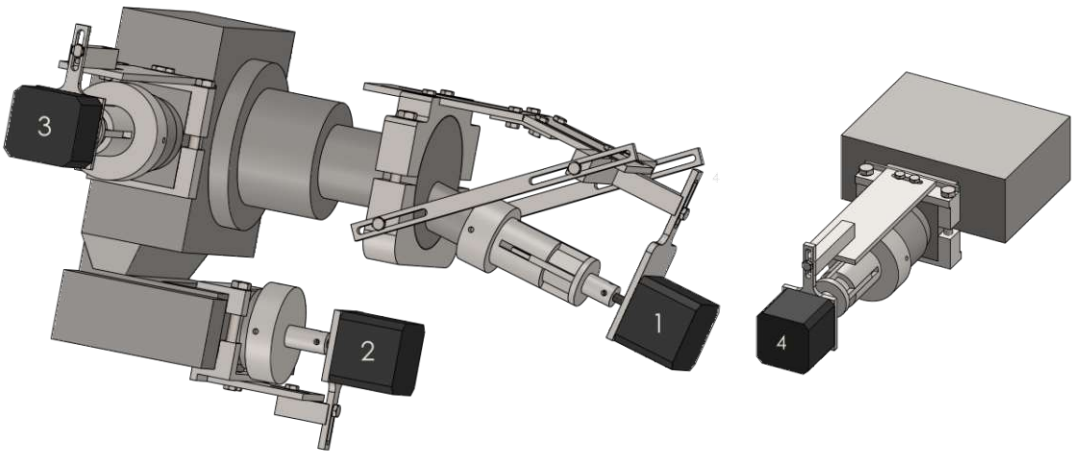

Figure 3.3.: Visualisation of the technical construction for the motorisation of the catcher manipulators (left) and the target manipulator (right); motor 1 rotates the catcher QCM around the y-axis, motor 2 moves the catcher QCM linearly in y-direction, motor 3 moves the catcher QCM linearly in x-direction, motor 4 moves the target QCM linearly in x-direction.

Subsequently, technical drawings of the individual components were prepared, and the single parts were manufactured in the IAP workshop. An overview of the constructional elements is attached in appendix B of this document.

Die approbierte gedruckte Originalversion dieser Diplomarbeit ist an der TU Wien Bibliothek verfügbar
The approved original version of this thesis is available in print at TU Wien Bibliothek.
TU Bibliothek Your knowledge hub WIEN

Motorisation and controlling

With the mounted construction, Nanotec ST4209M1206-A stepper motors could then be assembled onto these manipulators. The motors are connected to corresponding Nanotec SMCI33-2 motor controllers that are furthermore connected to a power supply. A RS485 port and a converting cable, establishing the communication between the controllers and the measurement computer, allow interaction with the controllers by sending digital commands. Firstly, a network of controllers has to be set up in order to be able to address different controllers for each motor. Once this network was implemented, I could then write executable Python scripts that can move specific motors in a defined way. More details on the executable Python scripts are illustrated by means of two exemplary applications for measurement routines explained in the next two sub-sections.

Figure 3.4 shows photos of the final motorised manipulators containing the assembled construction and the mounted stepper motors in our laboratory.

3.2.2. Automated target angle sweeps

As a rather straightforward but highly important measurement routine, the automated angle sweeps are presented. Here, the key procedure contains an irradiation of the target QCM under various angles of incidence. The individual experimental procedure steps are discussed below.

1. *A-priori* beam profile measurement

Before starting the measurement, the ion current density needs to be determined in order to be able to properly calculate the sputter yield based on equation (2.8). To this end, the FC, located at the bottom of the sample holder, can be used. By shortly stopping the irradiation by deflecting the beam in the Wien-filter, moving the FC into the beam and starting the irradiation again, a determination of the ion current density for the irradiated surface on the quartz is possible. It should be stressed that an appropriate beam scanning width, which sufficiently covers the sensitive area of the QCM, should be chosen.

Die approbierte gedruckte Originalversion dieser Diplomarbeit ist an der TU Wien Bibliothek verfügbar
The approved original version of this thesis is available in print at TU Wien Bibliothek.
TU Bibliothek Your knowledge hub WIEN

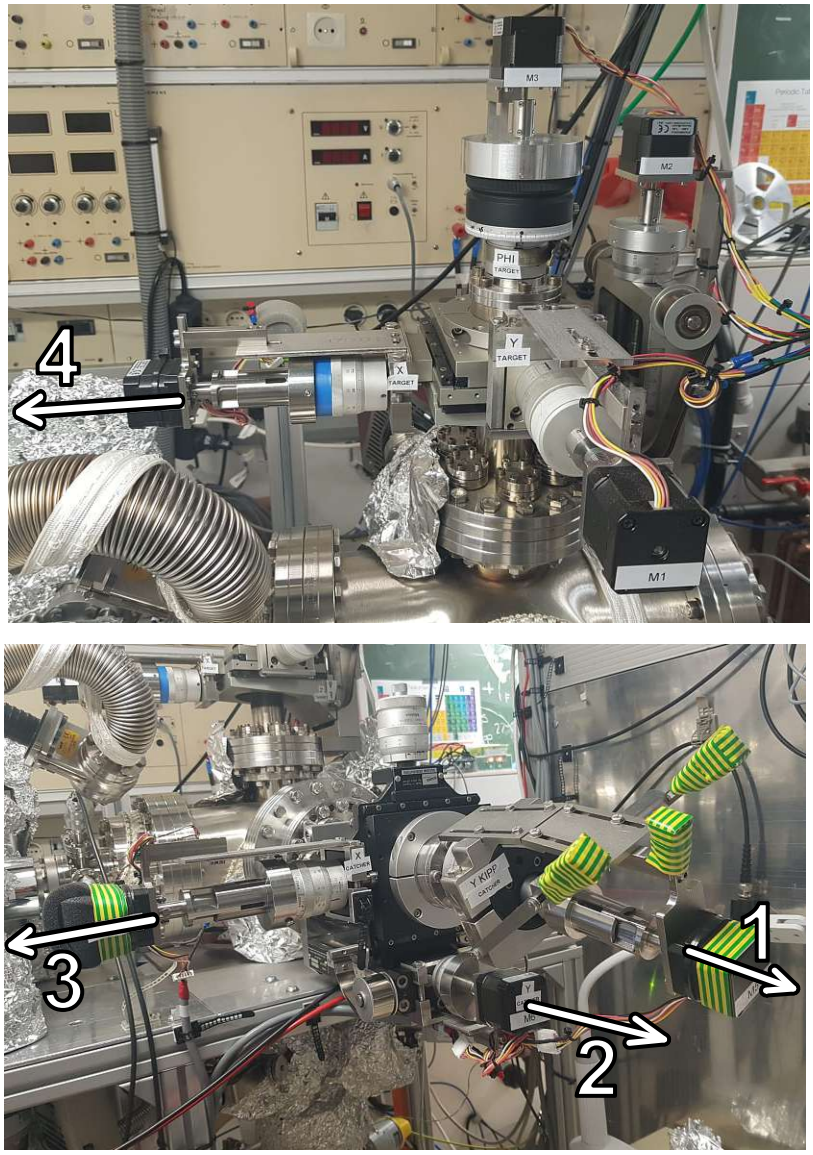

Figure 3.4.: Photo of the target QCM (top) and catcher QCM manipulators (bottom) with built-on constructional elements and motors. Axis 1 enables rotation of the catcher QCM around the x axis. Axis 2 corresponds to the catcher y direction. Axis 3 corresponds to the catcher x direction and axis 4 corresponds to the target x direction.

2. Sputter cleaning

Prior to the sweep, a sputter cleaning procedure is performed. Hence, one firstly irradiates the QCM sample in order to remove adsorbates and contaminations from the surface. The sputtering of weakly bound particles typically results in a large increase in the frequency signal, accounting for large $\Delta f/\Delta t$ values, which correspond to large sputter yields. As the contaminations are successively reduced in the process, the slope of

Die approbierte gedruckte Originalversion dieser Diplomarbeit ist an der TU Wien Bibliothek verfügbar
The approved original version of this thesis is available in print at TU Wien Bibliothek.
TU Bibliothek Your knowledge hub WIEN

the frequency signal decreases. Once the slope reaches a stationary value, it can be concluded that most of the weakly bound particles have already been removed. More precisely, a region is reached, where the amount of adsorbed particles due to the residual gas pressure equals the amount of constantly sputtered adsorbate atoms, yielding a constant frequency slope. Therefore, the remaining stationary frequency change corresponds to sputtering of the actual sample material. Depending on the utilised ion species and the residual gas pressure within the setup during operation, this usually takes about 10-30 minutes.

3. Reaching steady state conditions

Subject to the used projectile and target materials, other dynamic effects might occur when exposing a sample to ion irradiation for the first time. Especially for strongly penetrating ion types, as it is typically the case for D_2^+ ions, implantation processes gain importance. Since the QCM signal enables to deduce total mass differences only, a differentiation between implantation processes and erosion processes that occur simultaneously is not possible. In order to measure pure erosion rates it is therefore recommended to wait until potential implantation processes have saturated. This behaviour might appear in the signal as slight reduction of the frequency slope throughout several hours of irradiation. Once the implantation process is saturated, the frequency signal, again, shows a constant slope. This development depends strongly on the utilised ion type and is practically negligible for Ar^+ ions, but takes up to days of irradiation for D_2^+ ions. In this case, the experimenter has to assess at which point steady state conditions are reached.

Aditionally, I want to stress that it might be useful to perform a secondary beam profile measurement in case steps two and three required large time frames compared to the real measurement sweep, described in step four.

4. Target angle sweep

Finally, as soon as steady state conditions are reached and the ion current is determined, one can start the actual measurement procedure. Here, one chooses a fixed beam time and irradiates the sample under a specified angle of incidence. After this first angle step the irradiation is shortly interrupted and the target position is rearranged so that the next irradiation step occurs at a different angle of incidence. Once the beam time has been chosen, this procedure can be performed automatically until a final incidence angle is reached. For reproducibility, the procedure can then be reversed and incidence angles starting from the largest value down to normal incidence can be approached. In the course of this study, I performed a sweep using 5° steps and started from normal incidence approaching a final incidence angle of 70°. Afterwards, the procedure was reversed and subsequently angles starting from 70° to 0° were approached in 10° steps. It has to be mentioned, that 70° corresponds to the highest technically

Die approbierte gedruckte Originalversion dieser Diplomarbeit ist an der TU Wien Bibliothek verfügbar
The approved original version of this thesis is available in print at TU Wien Bibliothek.
TU Bibliothek Your knowledge hub WIEN

available rotation angle, due to mechanical constraints.
Note, that as the incidence angle ϕ increases, the area effectively being covered by the beam enlarges by a factor $1/\cos\phi$. It can therefore be useful, in order to prevent sputtering of the sample holder itself as well as to increase the signal, to reduce the beam scanning width as soon as one reaches a defined incidence angle threshold. This can also be considered by the automated routine developed in the course of this thesis. However, I want to stress that in this case also an additional beam profile measurement for the beam with reduced width is necessary.

5. *A-posteriori* beam profile measurement

In order to ensure that the beam intensity and cross section did not change severely during the experiment, it is necessary to perform an additional posterior beam profile. Hence, the beam has to be deflected shortly, before the FC is moved towards the irradiation position for a determination of the current density. This procedure is principally analogue to step number one. One can then use both a-priori and a-posteriori profiles to obtain a mean ion current density for the sputter yield calculation and additionally use the resulting standard deviation for a Gaussian error propagation to asses experimental errors.

6. Data post processing

Depending on the clarity of the detected signal, eventual post processing of the data might be needed. Data curation routines with the goal to exclude all but real mass effects from the recorded frequency data are twofold. One way is to exploit the dual mode technique as explained in section 2.3 in order to get rid of temperature effects in the frequency data. However, as this technique tends to be fragile and could possibly lead to larger errors, this might not always depict the optimal way of compensating unwanted effects. It therefore underlies the assessment of the experimenter if this technique is the best choice to enhance the quality of the raw data. Another method that at least partially filters out unwanted effects contains simple frequency drift compensations. Here, the idea is to use the frequency drift measured slightly before and shortly after an irradiation step, calculate a mean value of the two drift frequencies and subtract the quantity from actually measured frequency slopes during the irradiation. Both methods usually lead to data being more reproducible with less undesired temperature artefacts.

3.2.3. Automated catcher profiles

Subsequently, another important measurement technique that exploits the newly integrated manipulator motors is discussed. The key goal of the automated catcher profile experiments is to probe the angular distribution of sputtered particles (compare chapter

Die approbierte gedruckte Originalversion dieser Diplomarbeit ist an der TU Wien Bibliothek verfügbar
The approved original version of this thesis is available in print at TU Wien Bibliothek.
TU Bibliothek Your knowledge hub WIEN

2.2.2). Hence, the target QCM sample is irradiated conventionally at a certain angle, while the distribution of the released particles is measured with the catcher QCM, as indicated in the sketch shown in figure 2.2 in the previous chapter. Essentially, the position of the catcher QCM is altered in a discretised manner resembling a circular profile around the target.
It is mentionable that for such measurement routines an ion-target combination, which enables relatively high sputter yields, in order to ensure sufficiently large catcher signals, is necessary. For investigating W samples, utilising Ar^+ as projectile material is therefore a good choice. This additionally prevents the presence of possible dynamic phenomena happening in the beginning of an irradiation, arising from competing erosion and implantation processes.

1. Target sputter cleaning

Analogously to step two of the target angle sweep procedure, described in section 3.2.2, sputter cleaning of the target in order to remove weakly bound adsorbates from the surface is necessary. Since ion-target combinations resulting in comparably large sputter yields are used in this experimental routine, no prolonged effects but a relatively fast conversion towards steady state conditions is expected. Hence, this step typically takes about 10 minutes only.

2. *A-priori* beam profile measurement

Subsequently, a beam profile measurement to quantify the current density is needed in order to properly calculate the catcher yield during data analysis afterwards. The measurement procedure to probe the ion beam is fully analogue to the beam profile measurement described in step one of the target angle sweep routine in chapter 3.2.2.

3. Catcher sputter cleaning

In full analogy to the target sputter cleaning, the catcher QCM can also be cleaned from adsorbates by applying a sufficient Ar^+ fluence. Due to geometrical constraints in the experimental setup, resulting in large ion incidence angles when driving the catcher into the beam, catcher cleaning can in the case of this study be performed with reduced scanning in the horizontal direction.

4. Catcher pre-coating

Before finally starting the profile, it is necessary to wait for steady state conditions concerning the sticking of sputtered particles on the catcher surface. To this end, it is efficient to approach a preliminary catcher position and perform a pre-coating of the catcher.

Die approbierte gedruckte Originalversion dieser Diplomarbeit ist an der TU Wien Bibliothek verfügbar
The approved original version of this thesis is available in print at TU Wien Bibliothek.

This step is finished as soon as the catcher QCM frequency slope is constant, yielding equilibrium conditions. Generally, the most efficient angle step to be chosen for this purpose corresponds to a position, where it is known that the amount of sputtered particles into this direction is high. Typically, this is the case for the forward sputtering regime. However, also other positions that might fit better into the upcoming movements can be chosen, although it should be mentionend that the time used for pre-coating can in such cases be prolongated.
In this study, I used a pre-coating position of -15° with respect to the target surface normal and additionally applied W as both catcher and target material. Utilising this parameters, this step takes approximately 30 minutes.

5. Catcher profile

Finally, after steady state conditions are reached and the ion current has been determined, the actual measurement procedure can be started. A fixed beam time per irradiation step is set in a Python routine for automated catcher profile meaurements. For each step, the target QCM is irradiated under a fixed ion incidence angle (60° with respect to the target surface normal in the course of this study). After this beam time, the beam is shortly interrupted and the catcher QCM is moved towards the next discrete position on a circular track around the target. The frequency signal due to deposition of sputtered atoms is measured accordingly. This procedure is repeated until all discrete positions, which are selected in the automatisation Python routine, have been established.
In the course of this thesis, I followed angular interval steps along a circular path around the target QCM. The catcher QCM was moved using 5° and 7.5° steps between a starting position of -15° and a final position of 37.5° with respect to the target surface normal, as denoted as α in figure 2.2. For reproducibility, the path was reversed so that catcher positions were approached various times. A listing of the approached catcher positions specifically utilised in the course of this project is provided in appendix C.

6. *A-posteriori* beam profile measurement

The procedure of detecting the ion current density after the measurement then functions in full analogy to the preceding beam profile measurements. Probing the beam profile twice allows to assess whether the current stayed approximately constant during the experiment.

7. Data post processing

In analogy to the previously discussed target angle sweep, it might be necessary to perform post processing techniques to clean the data from unwanted temperature effects. However, utilising dual mode techniques was found to rather cause detrimental effects on the data quality when performing catcher measurements, due to relatively

Die approbierte gedruckte Originalversion dieser Diplomarbeit ist an der TU Wien Bibliothek verfügbar
The approved original version of this thesis is available in print at TU Wien Bibliothek.
TU Bibliothek Your knowledge hub WIEN

small catcher QCM signals and comparably large artifact creation during dual mode operation. Additionally, the catcher QCM movements performed during this procedure typically lead to unphysical spikes in the frequency signal, followed by a slow exponential decay. These effects might arise from mechanical stress applied on the quartz induced by the movement. Also, rearrangements of the cables and plug connections within the oscillating circuit can lead to fluctuations in the signal. Thus, compensating undesired effects by subtracting pre- and post-drifts in the frequency data for each irradiation step turned out to be a more efficient method in data post processing.

3.3. *In-situ* layer creation

When studying fusion relevant materials in general as well as redeposited layers thereof, it is favourable to create these redeposited layers *in-situ* in order to exclude possible alterations induced by exposure to air. Fortunately, with the twofold QCM setup it is possible to both erode and to create layers of material (in this case, W). For clarification, a slightly modified sketch of the twofold QCM setup, as already discussed in chapter 2.2.2, is shown in figure 3.5.

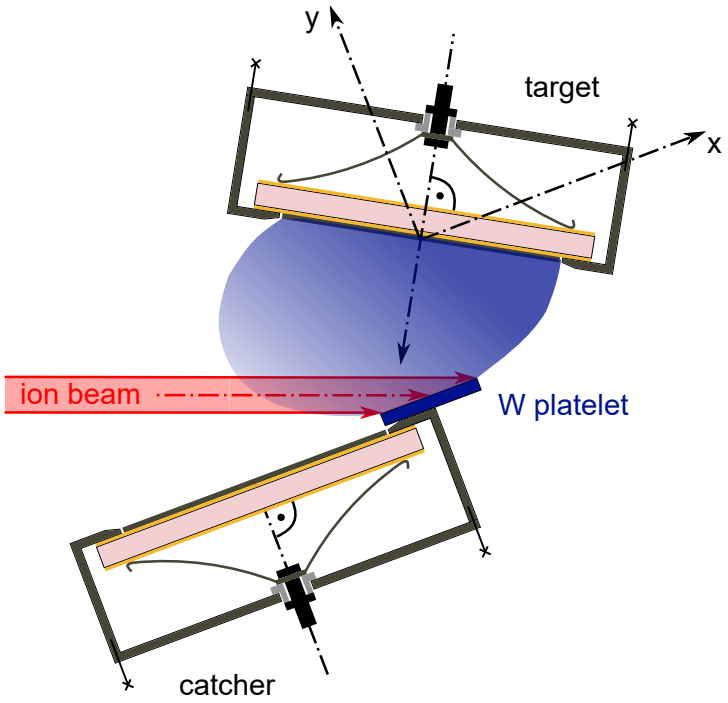

Figure 3.5.: Sketch of the twofold QCM setup, now containing also a W platelet localised on the edge of the catcher mount to enable *in-situ* W layer creations on the target QCM, adapted from [25].

Compared to figure 2.2, the catcher mount now hosts an additional W platelet, which

Die approbierte gedruckte Originalversion dieser Diplomarbeit ist an der TU Wien Bibliothek verfügbar
The approved original version of this thesis is available in print at TU Wien Bibliothek.

was installed within a previous project [35]. Target and catcher manipulators can be arranged in such a way, so that the ion beam hits the W platelet. The target quartz is then located in a position to catch the sputtered W particles and the precise growth rate can be monitored via the primary QCM. Thus, target and catcher roles can be reversed enabling layer creations on the target quartz *in-situ*. It should additionally be stressed, that it is useful to perform a sputter cleaning procedure, as described in chapters 3.2.2 and 3.2.3, on the W platelet before starting layer creations in order to remove adsorbates from the surface. More details on the *in-situ* layer creation methodology can be found in the outlined literature [35].

However, while this idea theoretically depicts an elegant way to create layers *in-situ*, due to the low ion flux in the setup and a subsequent low flux of W atoms reaching the target surface, the growth rates are rather small, settling in the range of $0.02 \cdot 10^{15}$ amu/cm^2/s. This corresponds to a rate of 17.46 fm/s or equivalently 1.52 nm/day, when assuming pure W growth. Creating nm-thick films is therefore time-consuming, occupying large amounts of machine time and even potentially resulting in wear outs of setup components, especially of the ion source and the Wien-filter.

Die approbierte gedruckte Originalversion dieser Diplomarbeit ist an der TU Wien Bibliothek verfügbar
The approved original version of this thesis is available in print at TU Wien Bibliothek.

4. Results and discussion

In the course of this study, two samples were utilised. Both samples consist out of a QCM quartz equipped with gold electrodes and a thin W layer on top that was eroded within the experiments. The W layers were created at the Max Planck Institute for Plasma Physics via magnetron sputtering [36]. Both W coatings were generated within the same batch using only one defined set of process parameters.

Firstly, a pure W sample was investigated. It is in the following referred to as 17W5 and was originally received from the Max Planck Institute for Plasma Physics and did not undergo any designed modifications at TU Wien. Secondarily, I utilised another pure W sample, labelled as 17W2. However, the secondary sample did indeed undergo modifications at TU Wien that are explained in more detail in the following subsections.

4.1. Pure tungsten sample

As an important first step, I took a look at the sputtering properties of pure W as target material. Prior to the sputter measurements, the surface of the sample was characterised via atomic force microscopy (AFM).

4.1.1. Sample characterization - AFM

Primarily, tapping-mode AFM was employed to characterise the morphology of the W coating on the quartz disk. Precisely, a Cypher S device from Oxford Instruments was used to obtain several images. Six pictures of 2x2 μm^2 size were taken in order to acquire satisfying statistics. An exemplary image, visualised using the software Gwyddion, is shown in figure 4.1 [37].

Die approbierte gedruckte Originalversion dieser Diplomarbeit ist an der TU Wien Bibliothek verfügbar
The approved original version of this thesis is available in print at TU Wien Bibliothek.
TU Bibliothek Your knowledge hub WIEN

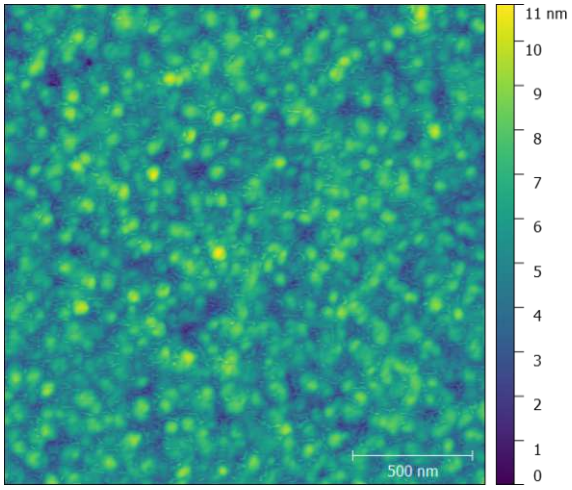

Figure 4.1.: AFM image of the pure W sample, 17W5.

It can be seen from figure 4.1 that the highest hillocks reach 11 nm only, therefore resembling a rather smooth mirrorlike surface.

4.1.2. 2 keV Ar^+ target angle sweep on pure W

In the next step, a target angle sweep measurement profile, as discussed in chapter 3.2.2, was performed. As in prospective fusion reactors, Ar will possibly be used as seeding gas in the divertor region, I firstly probed the sputtering behaviour of the sample via irradiation with Ar^+ ions accelerated at 2 keV kinetic energy [38]. The obtained data is shown in figure 4.2.

As the sputter yield for Ar^+ irradiation of W is relatively high, no data post processing was needed in this case, since the frequency changes were completely dominated by mass changes. Figure 4.2 therefore shows essentially sputter yields deduced from raw data, resembling the slopes of the recorded quartz eigenfrequency at each specific incidence angle. It can also be seen that, for reproducibility, several angular positions were approached repeatedly in a random order in order to allow identification of possible effects arising from long-term temperature fluctuations. As the individual data points are in very good agreement with each other, it can be concluded that no severe temperature variations have arisen during the measurement.

Die approbierte gedruckte Originalversion dieser Diplomarbeit ist an der TU Wien Bibliothek verfügbar
The approved original version of this thesis is available in print at TU Wien Bibliothek.

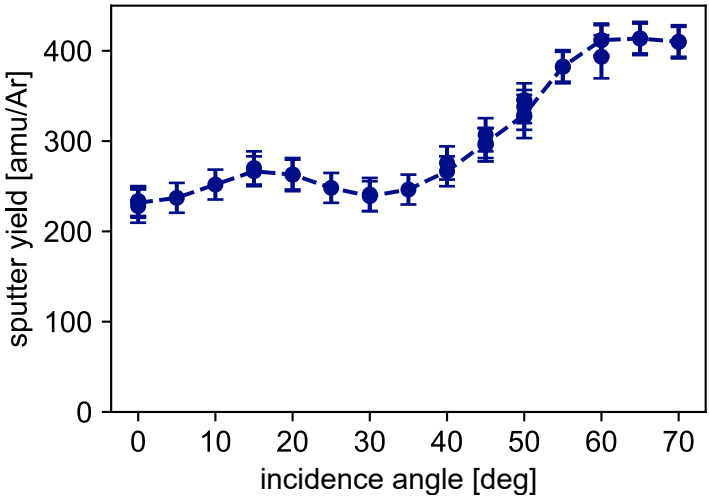

Figure 4.2.: Sputter yield as a function of the ion incidence angle under bombardment of the pure W sample, 17W5, with 2 keV Ar^+ ions.

Furthermore, I want to stress that the shown data points were obtained using two different beam scannings for different incidence angles. Namely, the beam scanning in the horizontal direction was reduced by a factor of two for incidence angles larger than 50° in order to firstly prevent sputtering of the sample holder itself and secondly to enlarge the measured frequency slope due to a more focused ion irradiation of the quartz center. Two individual sets of ion beam profiles for each scanning setting were considered for data analysis, which enabled perfect agreement of the data points measured at 50° incidence angle.

It can be seen that the sputter yield by trend rises as the inclination angle is increased. At normal incidence the yield starts at 228 amu/Ar and rises up to a maximum value of 414 amu/Ar at 65° incidence angle. The yield slightly decreases again after 65° resulting in 410 amu/Ar at 70°, the largest incidence angle during the experiment. However, a small decrease resulting in a local minimum at approximately 30° is visible in the shown data. From a physical point of view, such a local minimum is rather unexpected for sufficiently flat samples with amorphous or reasonably randomly oriented polycrystalline texture. Thus, possible hypotheses that could explain such properties are discussed in chapter 4.3 of this document.

4.1.3. 2 keV D_2^+ target angle sweep on pure W

Secondly, an even more fusion relevant ion species was utilised as projectile. I used D_2^+ ions, accelerated towards 2 keV kinetic energy, considering that D will function as part of the fusion fuel in future reactors. The automatic measurement routine, explained in chapter 3.2.2, was exploited. Obtained data are shown in figure 4.3.

Die approbierte gedruckte Originalversion dieser Diplomarbeit ist an der TU Wien Bibliothek verfügbar
The approved original version of this thesis is available in print at TU Wien Bibliothek.

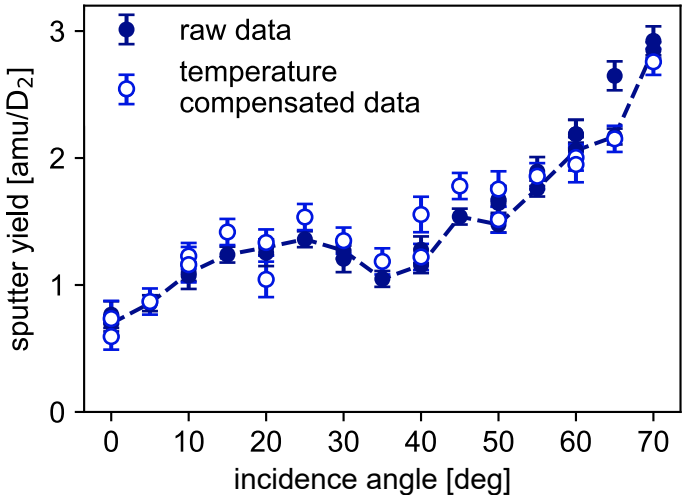

Figure 4.3.: Sputter yield as a function of the ion incidence angle under bombardment of the pure W sample, 17W5, with 2 keV D_2^+ ions.

What is apparent at first glance, is that the absolute values of the sputter yields are by orders of magnitude smaller, compared to the case using Ar as projectile. Precisely, the yield starts at 0.7 amu/D_2 and peaks at 2.9 amu/D_2 at the highest approached incidence angle of 70°. This behaviour can be explained by the different mass ratio between target and ion species, leading to different scattering kinetics and less energy transfer towards the target atoms. This results in lower sputter yields [21].

However, such small sputter yields complicate the experimental approach. Due to the filigree frequency changes observed during D_2^+ irradiation, even small temperature fluctuations can contribute severely to the measured frequency slope, leading to miscalculated sputter yields. In order to circumvent such systematic errors, this measurement was performed twice. On one hand, the experiment was performed by means of the classical single mode QCM technique and on the other hand by exploiting the dual mode procedure, as discussed in chapter 2.3. In both cases the individual angle steps were approached several times in order to be able to detect any further systematic errors. The data points obtained using the classical QCM mode, i.e. exciting solely the ground mode of the quartz and maintaining the oscillation in resonance, are visualised in figure 4.3 as dark blue dots. The lighter blue circles correspond to measurements obtained via exploiting the dual mode technique, i.e. by exciting quasi-simultaneously the quartz' ground and third mode. This technique *per se* leads to a higher risk of artifact creation, due to the persistent changing of oscillation modes. Therefore, while the dark blue data points follow a more concise trend, the lighter blue circles show more scatter, despite resembling a similar trend. This in turn allows to conclude that temperature effects did not severely influence the signals during this measurement. Therefore, the single mode data appear reliable enough.

Die approbierte gedruckte Originalversion dieser Diplomarbeit ist an der TU Wien Bibliothek verfügbar
The approved original version of this thesis is available in print at TU Wien Bibliothek.

In analogy to the measurement run described in 4.1.2, also in this case variable beam scannings were used for different incidence angles. Again, no deviation of the sputter yield at the interconnecting regime at 50° incidence angle is found.

Analogously to the data obtained for the 2 keV Ar^+ case (see chapter 4.1.2.), the sputter yield by trend enlarges as the incidence angle is increased, however showing a local minimum at about 35° incidence angle for D_2^+ bombardment. As already stated in the previous subsection, this minimum appears counterintuitive as long as sufficiently smooth and polycrystalline samples are considered. This issue will be tackled further in chapter 4.3.

4.1.4. Catcher profile of pure W

Not only sputter yields, but also the angular distribution of the sputtered particles is of interest when studying sputtering properties in general. Therefore, I additionally applied the catcher profile procedure, illustrated in chapter 3.2.3, using a pure W coating. Ar^+ was utilised as projectile and the sample was irradiated under 60° incidence angle, while the catcher was moved along a circular path around the target. The obtained data is shown in figure 4.4.

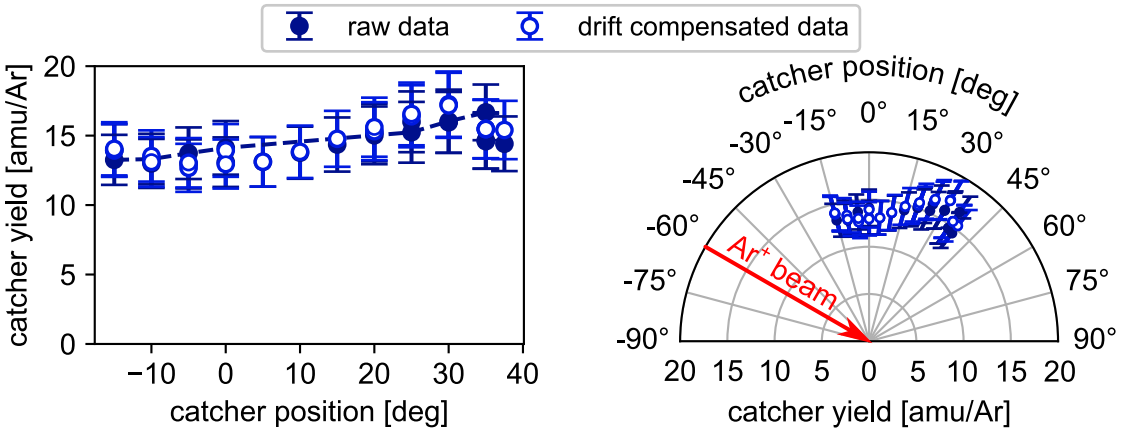

Figure 4.4.: Catcher yield as a function of the catcher position, relative to the surface normal of the pure W target, 17W5, which is under bombardment with 2 keV Ar^+ ions at an incidence angle of 60°. The data is visualised both as linear plot (left) and polar plot (right).

The left-hand side of figure 4.4 shows the data points visualised as linear plot, while the right hand side shows a polar plot of the same data, additionally indicating the direction of the incoming ion beam onto the target. The dark blue data points correspond to obtained raw data, whereas the lighter blue circles underwent post processing. As it was already discussed in section 3.2.3, it is rather uncommon to use dual mode techniques for such catcher profiles, due to the large artefacts caused by the sequential

Die approbierte gedruckte Originalversion dieser Diplomarbeit ist an der TU Wien Bibliothek verfügbar
The approved original version of this thesis is available in print at TU Wien Bibliothek.

mode switching. Still, data post processing via drift compensation can be performed. Hence, this method was conducted in this case. It can, however, be seen that raw and drift compensated data resemble each other well, supporting the assumption that no side-effects influenced the measurement. For reproducibility, individual catcher positions were approached repeatedly at different measurement times in order to enable detection of any chronological correlations or other systematic errors. As can be seen in figure 4.4, such dynamic effects can be excluded due to the satisfying agreement of the data trends.

The absolute catcher yields show values between 12 and 18 amu/Ar. The yield is slightly larger in the forward sputtering regime (at about 30°) than in the backward sputtering regime, which could be interpreted as a single knock-on peak [30].

4.1.5. Comparison to simulation results obtained via SDTrimSP

In order to compare the experimental data with simulation results, I additionally performed simulations using the code SDTrimSP, which was briefly discussed in chapter 2.4 [32]. The obtained findings for irradiation with both Ar^+ and D_2^+ are shown in figure 4.5.

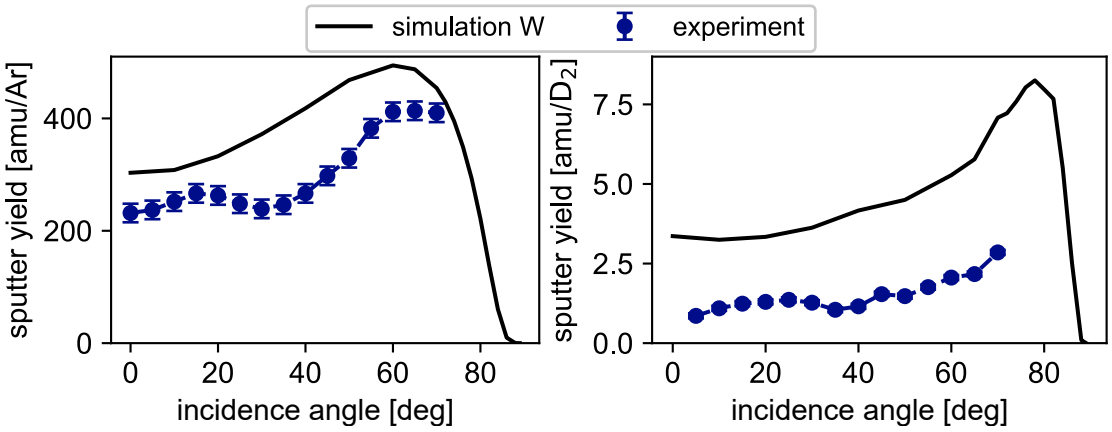

Figure 4.5.: Sputter yield as a function of the ion incidence angle under bombardment of W with 2 keV Ar^+ ions (left) and 2 keV D_2^+ ions (right): measured experimentally by QCM using the pure W sample, 17W5, (visualised as blue dots) and calculated via the simulation code SDTrimSP [32] (visualised as black solid line).

Concerning the simulation setup, I used 2 keV Ar^+ ions as projectiles and pure W with a default value of 8.79 eV for its surface binding energy as target material, in full analogy to the experiment. Furthermore a static simulation method and default settings for the integration method (Gauß-Legendre) and the interaction potential (Kr-C potential) were used, as they are the most prominently used parameters for such calculations in our research group. Data regarding the Ar^+ irradiation can be seen on the left side of figure 4.5.

Die approbierte gedruckte Originalversion dieser Diplomarbeit ist an der TU Wien Bibliothek verfügbar
The approved original version of this thesis is available in print at TU Wien Bibliothek.

Subsequently, also a simulation using D^+ as projectile material was performed. In order to resemble the experimental conditions, where I used 2 keV D_2^+ ions, now 1 keV D^+ ions for the simulation were utilised and the obtained sputter yield given in amu/D was then multiplied by a factor of 2, in order to mimic the yield in terms of amu/D_2. Obtained data is shown in the left panel of figure 4.5. It can be seen in both irradiation cases, that the absolute values show a certain offset. However, the general trend of increasing sputter yields for increasing the incidence angle up to a certain maximum is also recognisable in the simulated curve, visualised in both panels of figure 4.5 as black solid line. Nevertheless, no kinks or local minima are visible in the simulated curve.

4.2. Redeposited tungsten sample

As second step of this project, a redeposited layer was created *in-situ* in order to perform the exact same measurement procedures as the ones conducted before, concerning the original pure W layer. The layer creation was performed exploiting the twofold QCM setup, as explained in chapter 3.3. Hence, I implemented a QCM sample already hosting a W layer as target sample and grew further W on top of its surface.

4.2.1. Sample characterization - IBA and QCM

Since the layer creation occurred *in-situ* on the target QCM, a precise monitoring of the growth rate during the process was possible. As already outlined in section 3.3., however, the growth rates were rather low due to limitations of the setup, which is indeed not designed for growing layers of several nm. In total, an overall frequency decrease of 1199.3 Hz, corresponding to a mass increase of $9676.2 \cdot 10^{15}$ amu/cm^2, was obtained. Additionally, it should be stressed that the layer was created inside a D_2 environment by manually letting in D_2 gas into the experimental chamber in order to reach a pressure value of 10^{-5} mbar with the idea to mimic more reactor relevant conditions.

Nevertheless, as QCM signals can only be interpreted as net mass changes, no information concerning the elemental composition of the grown film can be deduced. Thus, additional analyses were necessary. The sample was therefore also investigated by means of ion beam analysis (IBA) at the Department of Physics and Astronomy at Uppsala University, Sweden. The obtained IBA data is shown in figure 4.6.

Die approbierte gedruckte Originalversion dieser Diplomarbeit ist an der TU Wien Bibliothek verfügbar
The approved original version of this thesis is available in print at TU Wien Bibliothek.
TU Bibliothek Your knowledge hub WIEN

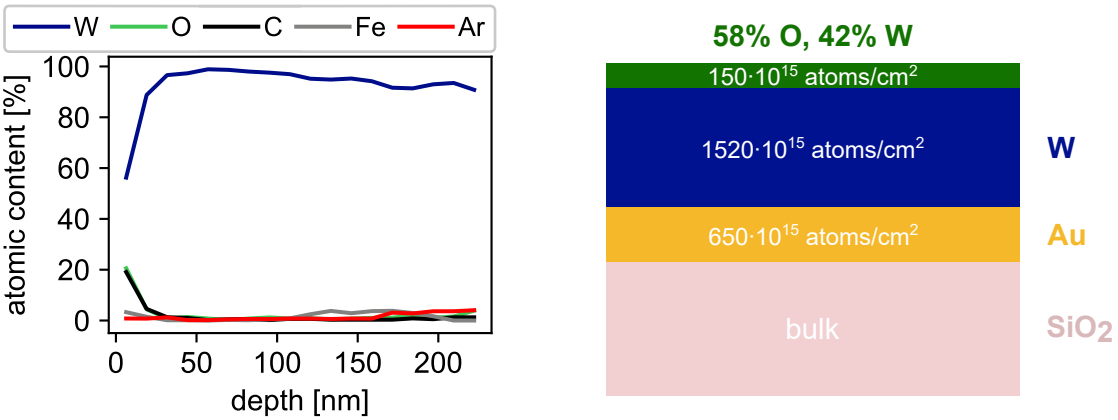

Figure 4.6.: Depth profile of the sample hosting a pure W layer and a redeposited WO layer, 17W2 + redeposited WO: Data obtained via a ToF-ERDA measurement using I^{8+} ions at 36 MeV under an incidence angle of 67.5° respective the surface normal and a detector position at 45° is shown in the left panel; Data obtained via a RBS measurement using He^{+} ions at 2 MeV under an incidence angle of 5° and a detector position of -5°, both respective the surface normal is shwon in the right panel.

At first, a time-of-flight elastic recoil detection analysis (ToF-ERDA) measurement was performed. To this end, the sample was bombarded with I^{8+} ions at 36 MeV under an incidence angle of 67.5° respective the surface normal direction. A detector located at 45° respective the sample surface normal in forward scattering direction was then used to detect scattered sample atoms. Analysing the energy and time dependent detector data allows to compute the elemental composition of the investigated target [39, 40].

Visible in the left panel of figure 4.6, the considered sample hosts predominantly W and small amounts of impurities, namely O, C, Fe, and Ar, which make up less than 10% of the bulk composition. Directly at the surface, the contributions from O and C are larger and make up 20% each, yielding a W concentration of only 60% at the surface.

However, as the depth resolution of this method is relatively low and the redeposited layer was comparably thin, a secondary ion beam analysis method was applied, namely Rutherford backscattering spectrometry (RBS). In the course of this, He^{+} ions at 2 MeV under an incidence angle of 5° to the surface normal were shot at the target surface and the backscattered ions were analysed within a detector at an angular position of -5°, relative to the surface normal of the target. This technique is also capable to enable insights into the sample composition. The corresponding data is shown schematically in the right panel of figure 4.6. The top layer, consisting of both W and O, revealed a thickness of $150.0 \cdot 10^{15}$ atoms/cm^2. By using the determined elemental composition of 58% O and 42% W, this yields a total mass areal density of this film of $12971.4 \cdot 10^{15}$ amu/cm^2. This is indeed comparable to the total mass increase measured by QCM, which was determined as $9676.2 \cdot 10^{15}$ amu/cm^2. The remaining difference of 25% might have arisen from spatially inhomogeneous coating conditions, which can be relevant if the

Die approbierte gedruckte Originalversion dieser Diplomarbeit ist an der TU Wien Bibliothek verfügbar
The approved original version of this thesis is available in print at TU Wien Bibliothek.
TU Bibliothek Your knowledge hub WIEN

probing He^+ beam eventually has hit the sample at a peripheral spot, where the layer was slightly thicker.

While it was originally intended to create a redeposited W film, it can be seen from both plots in figure 4.6 that the grown layer contains indeed a lot of oxygen, and the film can therefore be interpreted as a WO layer. This fact should, however, not appear counter-intuitive, as the deposition rates during layer growth were small and even small amounts of residual gases can adsorb during the process. Furthermore, due to the low depth resolution, a distinction between a homogeneous distribution of W and O in the redeposited film, or a structure consisting of a pure W layer with adsorbates on top, can hardly be made. At this point, it is important to mention that the sample was transported under atmosphere to Uppsala University. The *in-situ* approach was therefore lost in order to enable elemental characterisation of the sample.

Secondly, it should be noted at this point that the used QCM sample for creating the redeposited layer and the subsequent sputtering measurements was different to the one used for the investigation of pure W. However, as stated in the beginning of this chapter, the two samples, 17W5 and 17W2, were created using the same process parameters and can be assumed to host analogue W coatings.

4.2.2. 2 keV Ar^+ target angle sweep on redeposited WO

After characterising this sample, I could then repeat the experimental procedures that were already used for the pure W layer. Therefore, a first target angle sweep measurement using Ar^+ ions at 2 keV as projectiles was performed. The exact same procedure as illustrated in chapter 4.1.2. and explained in section 3.2.2. was utilised. However, due to the thin film and the elemental composition, which might lead to dynamic changes of the composition and a general quick erosion of the film, special attention during the procedure was demanded. While a fluence that is large enough to reach stable conditions needed to be applied, it needed to be ensured that the redeposited film was not eroded entirely. To this end, preceding dynamic simulations exploiting SDTrimSP ([32]) were performed in order to get a rough estimate of how large the applied fluences would need to be. The subsequently measured data are shown in figure 4.7.

Die approbierte gedruckte Originalversion dieser Diplomarbeit ist an der TU Wien Bibliothek verfügbar
The approved original version of this thesis is available in print at TU Wien Bibliothek.
TU Bibliothek Your knowledge hub WIEN

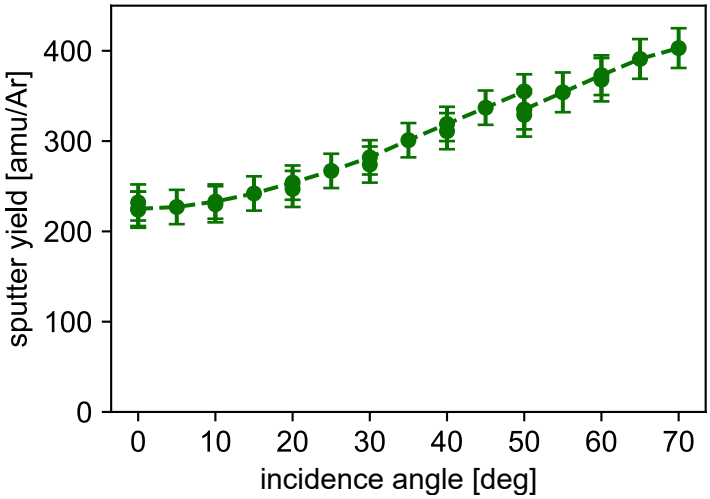

Figure 4.7.: Sputter yield as a function of the ion incidence angle under bombardment of the redeposited WO samplec, 17W2 + redeposited WO, with 2 keV Ar^+ ions.

The signal detected during the experiment was sufficiently high so that no post processing was needed and the dark green data points in figure 4.7 show essentially sputtering yields deduced from raw data. Analogously to the pure W case, some angle steps were approached repeatedly.

Furthermore, I again used two different beam scanning widths for different angle steps in full analogy to the method used previously. Whereas no deviations at 50° incidence angle were visible for the previously discussed target angle sweeps for the cases of Ar^+ on pure W and D_2^+ on pure W, a small offset is visible for the case shown in figure 4.7. However, this does not appear problematic, as this deviation lies fully within the error bars and might reflect the imperfect stability of the utilised ion current or a possible asymmetric irradiation for these beam scanning settings.

It can be seen that the sputter yield by trend increases as the inclination angle is enlarged, starting at a sputter yield of 225 amu/Ar at normal incidence and peaking at 403 amu/Ar at the largest approached angle of 70°. Interestingly, the local minimum that has been seen in the previous experiments for incidence angles of approximately 30° did no longer show up in this case.

4.2.3. 2 keV D_2^+ target angle sweep on redeposited WO

In full analogy to experiments on the pure W sample (compare chapter 4.1.3), a target angle sweep using D_2^+ ions at 2 keV as projectiles was performed. I consistently exploited the automatic measurement procedure explained in chapter 3.2.3. The obtained results are shown in figure 4.8.

Die approbierte gedruckte Originalversion dieser Diplomarbeit ist an der TU Wien Bibliothek verfügbar
The approved original version of this thesis is available in print at TU Wien Bibliothek.

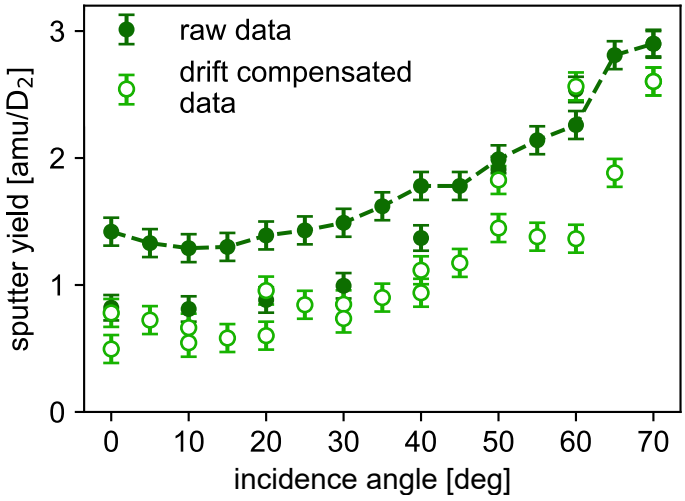

Figure 4.8.: Sputter yield as a function of the ion incidence angle under bombardment of a redeposited W sample with 2 keV D_2^+ ions.

It can be seen that in good agreement to the data obtained using the pure W sample, the sputter yield is by orders of magnitude smaller using D_2^+ as projectile, compared to Ar^+. The measured values for the sputter yields lie within a range between 0.5 amu/D_2 and 2.9 amu/D_2, as can be seen in figure 4.8. Experimental difficulties can be expected during measurements of such small sputter yields. Indeed, the obtained raw data, visualised as dark green dots in figure 4.8, show disagreement for some sputter yields, which were measured for reproducibility. In fact, the data points acquired with largest time difference show the most pronounced deviation. This in turn suggests that there was a slowly decaying long-term background drift present during the measurement, wich was probably caused by a laboratory temperature variation. Since the dual mode technique was in this case considered not to be the perfect choice due to the aforementioned challenges, the decided choice of data post-processing was the drift compensation approach. The compensated data are shown as lighter green data circles in figure 4.8. Even though a larger scatter was induced, the reproducibility of the data was improved.

It has to be mentioned that in this measurement run, no variation of the ion beam scanning was performed. The width of the scanning field therefore remained fixed with the aim to exclude diametral influences from the measurement. This was decided after the evaluation of results shown in chapter 4.2.2, where the scanning variation led to a small deviation visible at the interconnecting angular step of 50°.

As expected, no visible offsets were therefore found. In agreement with the data obtained by Ar^+ irradiation of this sample, no local minima can be recognised in the data shown in figure 4.8. However, the general trend of increasing yields by enlarging the incidence angle is again recognised. Further analysis of potential reasons for the absence

Die approbierte gedruckte Originalversion dieser Diplomarbeit ist an der TU Wien Bibliothek verfügbar
The approved original version of this thesis is available in print at TU Wien Bibliothek.

of a local minimum in this data is outlined in section 4.3 of this document.

4.2.4. Catcher profile of redeposited WO

As last experimental run, I subsequently performed a catcher profile via the procedure described in section 3.2.3. I consistently irradiated the target surface using Ar^+ ions at 2 keV under 60° incidence angle. The catcher QCM was driven around the target following a circular path. The obtained results are shown in figure 4.9.

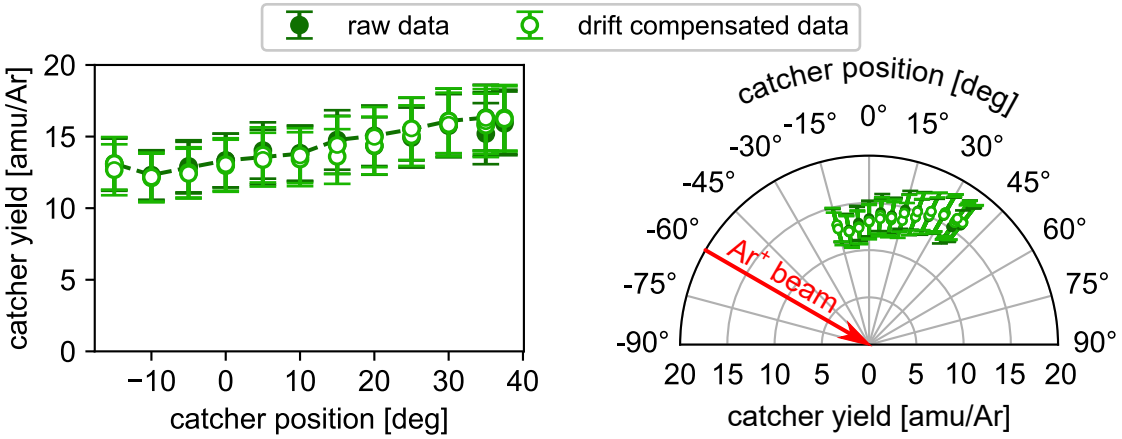

Figure 4.9.: Catcher yield as a function of the catcher position, relative to the surface normal of the redeposited WO sample, 17W2 + redeposited WO, which is under bombardment with 2 keV Ar^+ ions at an incidence angle of 60°. The data is visualised both as linear plot (left) and polar plot (right).

In full analogy to the pure W case (compare chapter 4.1.4), the left panel of figure 4.9 shows the data points visualised as linear plot, while the right-hand side illustrates a polar view. The dark green data points correspond to catcher yields deduced from the QCM raw data, while the lighter green circles represent drift compensated values. It can be seen that the drift compensated values resemble the raw data based values quite well, suggesting that no severe background drifts occurred during the measurement. Many angle positions were approached several times for reproducibility in order to circumvent possible systematic errors in the process.

It can be concluded that similarly to the pure W case, the absolute catcher yields appear to lie between 12 and 16 amu/Ar. A slight increase can again be seen in the forward sputtering regime, i.e. at angles of about 30° and langer, whereas the backward sputtering regime, i.e. emergent angles of 0° and less, is weakly suppressed [30].

I additionally want to stress that during this last experimental procedure, the applied Ar^+ fluence exceeded a threshold value, deduced by SDTrimSP ([32]), above which it is no longer guaranteed that the redeposited WO layer has not already been fully

Die approbierte gedruckte Originalversion dieser Diplomarbeit ist an der TU Wien Bibliothek verfügbar
The approved original version of this thesis is available in print at TU Wien Bibliothek.

eroded. However, data points that were obtained at later times during the experiment, corresponding to larger fluences already applied onto the target, coincide well with data points obtained in the beginning of the experiment. It is therefore assumable that the redeposited WO layer was not fully eroded prior measurement start and therefore this congruence supports the hypothesis that no dynamic processes, i.e. a shift from the redeposited WO to the subjacent pure W layer, occurred during the procedure.

4.2.5. Comparison to simulation results obtained via SDTrimSP

Furthermore, simulations via SDTrimSP ([32]) were performed as well for the case of irradiation of a WO surface. Firstly, I used 2 keV Ar^+ ions as projectiles to irradiate a WO target surface, containing 58% O and 42% W, respectively in this simulation. Additionally, default models and a surface binding energy of 8.79 eV for W and 1.00 eV for O were used.

Subsequently, simulated sputtering of a WO surface using D^+ ions was performed. Analogously to the procedure outlined in chapter 4.1.5, D^+ ions with 1 keV kinetic energy for the simulation were used. Thereafter, the obtained sputter yields in units of amu/D were multiplied by a factor of two to obtain amu/D_2. The simulated results, compared to the experimental data for both irradiation cases, are shown in figure 4.10.

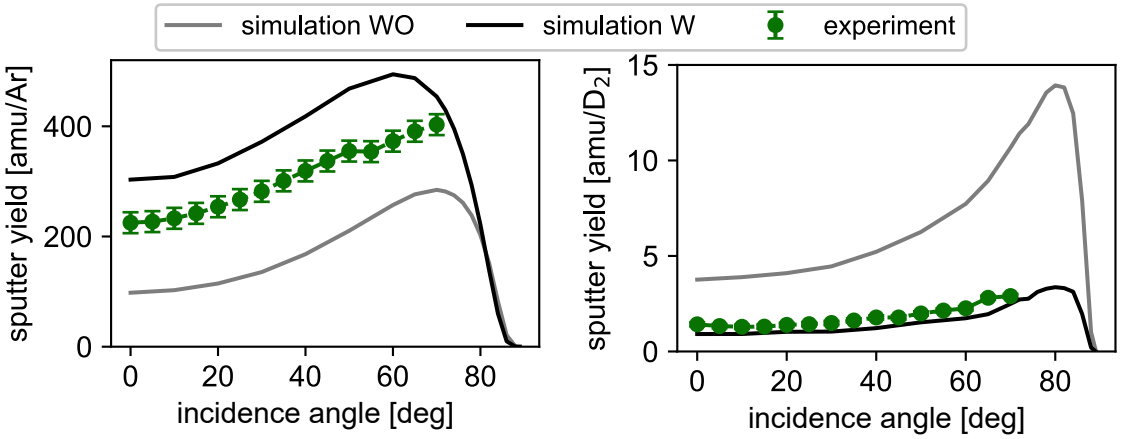

Figure 4.10.: Sputter yield as a function of the ion incidence angle under bombardment of WO with 2 keV Ar^+ ions (left) and 2 keV D_2^+ ions (right): measured experimentally by QCM using the redeposited WO sample, 17W2 + redeposited WO, (visualised as green dots) and calculated via the simulation code SDTrimSP [32] (visualised as grey solid line). For comparison also simulated data for irradiation of pure W is shown in the plots (visualised as black solid line).

Again, an offsets between experimental, depicted as green dots, and simulated data, visualised as solid lines, are visible in figure 4.10. The shown plots contain for comparison not only the simulation data using a WO surface but also the simulated data obtained for a pure W target. While there are offsets visible, it can be seen that in both irradiation cases, the simulation curve corresponding to pure W irradiation matches the

Die approbierte gedruckte Originalversion dieser Diplomarbeit ist an der TU Wien Bibliothek verfügbar
The approved original version of this thesis is available in print at TU Wien Bibliothek.

experimental data points better than the obtained data for a WO target. This gives rise to the hypothesis that the considered WO layer could possibly have rather resembled a structure consisting of a pure W layer with adsorbates on top than a homogeneous distribution of W and O in the redeposited film. However, it should be mentioned that offsets between experiment and simulation might as well rise from the fact that only a static calculation was performed within the simulation process. Therefore, possible preferential sputtering effects that would saturate with time are not presented by the simulated data [41]. Hence, this discrepancy might diminish by extending the simulation towards a dynamical method. Additionally, readjusting the surface binding energies of the target components could possibly lead to better agreement between experiment and simulation [30]. However, more detailed investigations requiring further analyses are beyond the scope of this project.

4.3. Discussion

The obtained data, shown in detail in sections 4.1 and 4.2, reveal interesting physical findings. Especially when comparing the sputtering behaviour of the two different target samples, pure W (17W5) and redeposited WO (17W2 + redeposited WO), respectively, the qualitative differences can be observed more clearly. Combined plots containing sputter yields in terms of amu/ion are shown in figure 4.11.

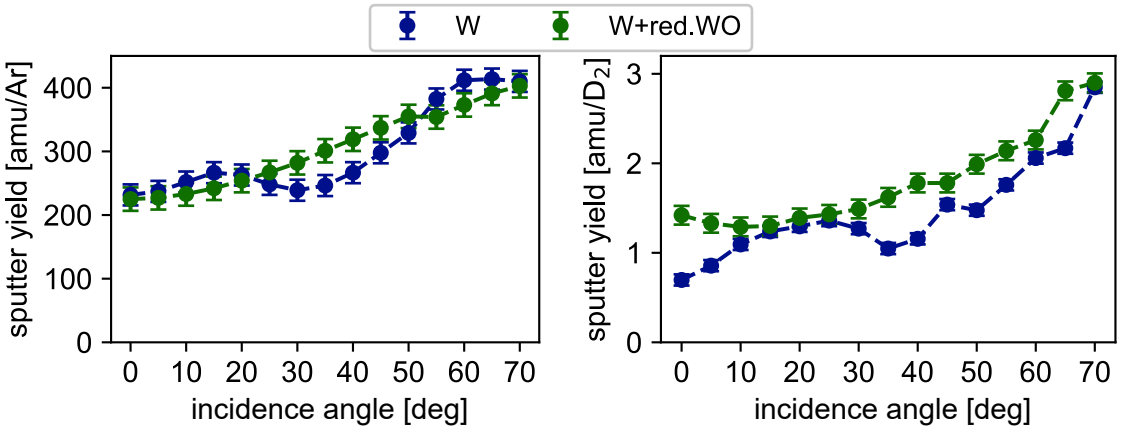

Figure 4.11.: Comparison of the angular dependent sputter yield for the pure W sample, 17W5, and the redeposited WO sample, 17W2 + redeposited WO, under 2 keV Ar^+ (left) and 2 keV D_2^+ (right) bombardment.

The left-hand side of figure 4.11 shows the case for 2 keV Ar^+ irradiation, while the right hand side visualises 2 keV D_2^+ irradiation. It is clearly visible that, while the data obtained for pure W shows a local minimum at about 30° to 35° angle of incidence for both

Die approbierte gedruckte Originalversion dieser Diplomarbeit ist an der TU Wien Bibliothek verfügbar
The approved original version of this thesis is available in print at TU Wien Bibliothek.

irradiation cases, data for the redeposited WO case resemble rather smoothly increasing sputter yields without any local minima. The absolute values of the sputter yield, however, are comparable to each other.

Firstly, this is an important information from the fusion point of view, as originally the question was addressed if sputtering properties of redeposited material are crucially different from the one of original layers. Disregarding the small local minima in the angular dependent sputter yield curves, the absolute values as well as the angular distribution of sputtered particles, measured with the QCM catcher, are very similar, when comparing original W and redeposited WO layers. A comparison of the angular distribution of sputtered particles is shon in figure 4.12. It can be seen that the individual distributions, where data corresponding to pure W are visualised in blue and data corresponding to redeposited WO are shown in green, are in good aggreement with each other.

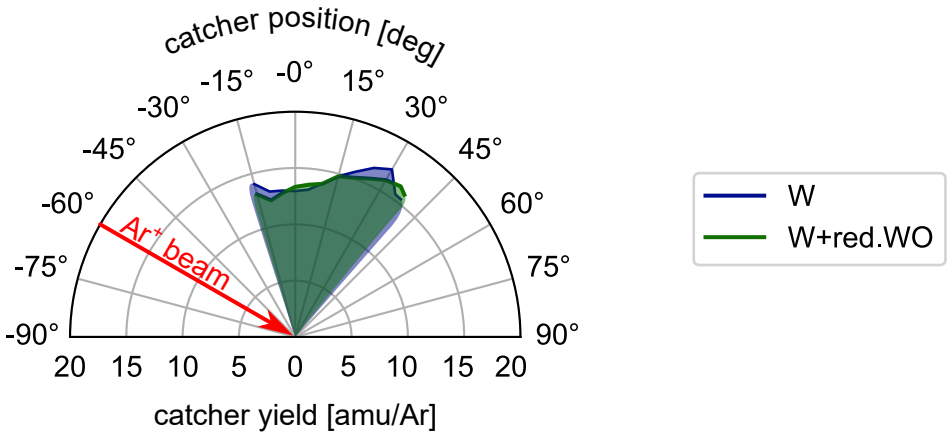

Figure 4.12.: Comparison of the angular distribution of sputtered particles from the pure W sample, 17W5, and the redeposited WO sample, 17W2 + redeposited WO, under ion bombardment under 60° incidence angle with 2 keV Ar^+ ions.

Secondly, if one takes a more detailed look at the angular dependence of sputter yields, the disappearance of the local minima deserves further analysis. A possible hypothesis that could explain the measured data is to assume a crystalline texture with a specific predominant direction. A non-randomly oriented polycrystalline surface could explain, why sputter yields at certain angle values between 0° and 60° appear smaller. The effect of a reduced sputter yield at a certain incidence angle due to a crystalline texture of a sample is called channeling. Here, the ions can travel through channels of a regularly oriented crystal structure with a much reduced probability for nuclear scattering events. The penetration depth of ions impinging along these channels is much larger than it would be the case for amorphous solids or unfavourable crystal orientations. Therefore, collision cascades are tendentially triggered much deeper in the solid, which reduces the chance for sputtering events. This results in a suppressed amount of released particles corresponding to lower sputter yields [42].

Die approbierte gedruckte Originalversion dieser Diplomarbeit ist an der TU Wien Bibliothek verfügbar
The approved original version of this thesis is available in print at TU Wien Bibliothek.

One way to investigate this issue further is to probe the crystal structure of the sample by, e.g., X-ray diffraction spectrometry (XRD) [43]. Qualitative measurements on the samples using XRD have already been performed at the X-Ray Center at TU Wien. Preliminary outcomes have shown that, in fact, the sample structure of the pure W sample, 17W5, deviates from a randomly oriented polycrystal. While a quantitative analysis is already ongoing, the hypothesis of a polycrystalline surface with preferred orientation is supported by the qualitative results, at least for this specific sample. However, the full quantitative study of the XRD data and follow-up numerical simulations exceed the scope of this thesis.

Moreover, other conducted QCM experiments, although not relevant for the central theme of this project, revealed a similar behaviour concerning Fe samples. These samples were produced in the same facility within the same year as the investigated W coatings. Therefore, this depicts another indication that indeed channelling effects might have been present in the investigation, highlighting the capabilities of our experimental setup also for such a scope of studies.

Die approbierte gedruckte Originalversion dieser Diplomarbeit ist an der TU Wien Bibliothek verfügbar
The approved original version of this thesis is available in print at TU Wien Bibliothek.

5. Conclusion and outlook

In the course of this thesis, a precise QCM measurement technique to investigate sputtering properties of W model systems relevant for nuclear fusion devices has successfully been applied. The used setup at the Augustin laboratory at IAP TU Wien has been upgraded for this task. Precisely, additional stepper motors in order to enable remote control of crucial manipulator axes were implemented. These upgrades furthermore allow to run more sophisticated measurement procedures without time constraints and substantially reduce human time resources on site. In fact, the experimental setup has therefore been fully automated, generally liberating the experimental procedures.

Subsequently, the upgraded setup has been used to investigate sputtering properties of a pure W coating, as well as of a similar sample hosting additionally a redeposited WO layer in the range of a few nm. Briefly, while the absolute sputter yield values of original and redeposited layers as well as their angular dependence of emitted particles are comparable, interesting differences can be found when taking a closer look onto the angular dependent sputter yields for incidence angles around 30° to 35°. In this regime it was shown that the pure W sample revealed smaller sputter yields than it was the case for redeposited material. This issue was furthermore investigated qualitatively, by means of XRD, resulting in the hypothesis that channelling effects have played a role for the detected sputter yield variations. Surely, a quantitative analysis of the suggested channelling effects requires further effort and poses a potential outlook. Additionally, it should be stressed that occurred limitations, such as low growth rates during layer creations and the need for *ex-situ* sample transport for IBA, impose issues that can be tackled in the future, yielding even more accurate measurement procedures. These points limit clear conclusions of the elemental composition of the very thin redeposited layer, which might have been just a composition of a W base layer with adsorbate coverage. This could explain the shown similarity of the sputtering data regarding the redeposited layer with the pure W cases. However, the exploited QCM technique together with our fully automated measurement setup illustrate a highly powerful experimental tool and provide a good basis for future studies to come.

Concludingly, even though small deviations between the two considered samples, pure W and redeposited WO, were found, the general sputtering characteristics are similar. These deviations, however, might be attributed to the aforementioned channeling effects. Therefore, from the perspective of erosion of redeposited material on first wall parts, no issues are to be expected for future fusion reactor devices.

Die approbierte gedruckte Originalversion dieser Diplomarbeit ist an der TU Wien Bibliothek verfügbar
The approved original version of this thesis is available in print at TU Wien Bibliothek.
TU Bibliothek Your knowledge hub WIEN

References

1. C. Cupak et al. Sputter yields of rough surfaces: Importance of the mean surface inclination angle from nano-to microscopic rough regimes. *Applied Surface Science* **570,** 151204 (2021).
2. C. Watzenböck et al. Long-term memory magnetic correlations in the Hubbard model: A dynamical mean-field theory analysis. *arXiv preprint arXiv:2112.02903* (2021).
3. A. Lopez-Cazalilla et al. Comparative study regarding the sputtering yield of nano-columnar tungsten surfaces under Ar^{+} irradiation. (submitted, 2022).
4. F. A. Hernández et al. First principles review of options for tritium breeder and neutron multiplier materials for breeding blankets in fusion reactors. *Fusion Engineering and Design* **137,** 243–256 (2018).
5. L. Rodríguez-Penalonga et al. A review of the nuclear fuel cycle strategies and the spent nuclear fuel management technologies. *Energies* **10,** 1235 (2017).
6. ITER. Official Website. https://www.iter.org/ (accessed 10.05.2021).
7. Eurofusion. Official Website. https://www.euro-fusion.org/news/2022/european - researchers-achieve-fusion-energy-record/ (accessed 26.02.2022).
8. T. Casper et al. Development of the ITER baseline inductive scenario. *Nuclear Fusion* **54,** 013005 (2013).
9. Jet Team et al. Fusion energy production from a deuterium-tritium plasma in the JET tokamak. *Nuclear Fusion* **32,** 187 (1992).
10. W. M. Stacey. *Fusion: An introduction to the physics and technology of magnetic confinement fusion.* John Wiley & Sons (2010).
11. J. Linke. High heat flux performance of plasma facing materials and components under service conditions in future fusion reactors. *Fusion science and technology* **49,** 455–464 (2006).
12. R. Behrisch. First-wall erosion in fusion reactors. *Nuclear Fusion* **12,** 695 (1972).
13. R. Neu et al. Overview on plasma operation with a full tungsten wall in ASDEX Upgrade. *Journal of Nuclear Materials* **438,** S34–S41 (2013).
14. R. Stadlmayr et al. A high temperature dual-mode quartz crystal microbalance technique for erosion and thermal desorption spectroscopy measurements. *Review of Scientific Instruments* **91,** 125104 (2020).
15. M. Rubel et al. Application of Ion Beam Analysis in Studies of First Wall Materials in Controlled Fusion Devices. *Physics* **4,** 37–50 (2022).

Die approbierte gedruckte Originalversion dieser Diplomarbeit ist an der TU Wien Bibliothek verfügbar
The approved original version of this thesis is available in print at TU Wien Bibliothek.
TU Bibliothek Your knowledge hub WIEN

16. G. Sauerbrey. Verwendung von Schwingquarzen zur Wägung dünner Schichten und zur Mikrowägung. *Zeitschrift für Physik* **155,** 206–222 (1959).
17. G. Hayderer et al. A highly sensitive quartz-crystal microbalance for sputtering investigations in slow ion–surface collisions. *Review of scientific instruments* **70,** 3696–3700 (1999).
18. M. Schmid. *Möglichkeiten und Grenzen der Schwingquarz-Schichtdickenmessung.* Doctoral Dissertation. TU Wien (1989).
19. P. S. Szabo. *Experimental and Simulated Sputtering of Gold, Iron and Wollastonite with a Catcher-QCM Setup.* Master thesis. TU Wien (2017).
20. P. S. Szabo. *Novel Insights into Ion-Solid Interaction: Case Studies for Space Weathering and Nuclear Fusion Research.* Doctoral Dissertation. TU Wien (2021).
21. P. Sigmund. Sputtering by particle bombardment theoretical concepts. *Topics in applied physics* **47,** 9 (1981).
22. B. M. Berger. *Laboratory work on plasma-wall-interaction processes relevant for fusion experiments.* Doctoral Dissertation. TU Wien (2017).
23. R. Stadlmayr. *Erosion of fusion relevant materials-experiments and modelling.* Doctoral Dissertation. TU Wien (2020).
24. B. M. Berger et al. Sputtering measurements using a quartz crystal microbalance as a catcher. *Nuclear Instruments and Methods in Physics Research Section B: Beam Interactions with Materials and Atoms* **406,** 533–537 (2017).
25. C. Cupak. *Influence of Roughness on Sputter Yields of Tungsten Coatings relevant for Nuclear Fusion Devices.* Master thesis. TU Wien (2019).
26. L. Bachmann et al. Measurement of the sticking coefficients of silver and gold in an ultrahigh vacuum. *Journal of Applied Physics* **37,** 242–246 (1966).
27. D. E. Pierce et al. A temperature insensitive quartz microbalance. *IEEE transactions on ultrasonics, ferroelectrics, and frequency control* **45,** 1238–1245 (1998).
28. M. Fellinger. *A QCM Performance Analysis with focus on Dual Mode Measurements.* Project report. TU Wien (2021).
29. M. T. Robinson. The binary collision approximation: Background and introduction. *Radiation Effects and Defects in Solids* **130,** 3–20 (1994).
30. H. Hofsäss et al. Simulation of ion beam sputtering with SDTrimSP, TRIDYN and SRIM. *Applied Surface Science* **310,** 134–141 (2014).
31. M. Bear et al. Atomic and Ion Collisions in Solids and at Surfaces: Theory, Simulation and Applications. *American Scientist* **86,** 188 (1998).
32. A. Mutzke et al. SDTrimSP Version 6.00. Max-Planck-Institut für Plasmaphysik (2019).
33. P. S. Szabo et al. Graphical user interface for SDTrimSP to simulate sputtering, ion implantation and the dynamic effects of ion irradiation. (submitted, 2022).

Die approbierte gedruckte Originalversion dieser Diplomarbeit ist an der TU Wien Bibliothek verfügbar
The approved original version of this thesis is available in print at TU Wien Bibliothek.
TU Bibliothek Your knowledge hub WIEN

34. A. Redl. *Creation of a Python-based control software for QCM measurements and implementation of a real-time GUI for data acquisition.* Project report. TU Wien (2022).
35. J. Filzmoser. *Upgrade of an experimental setup for investigation of D retention through sputter-depostited W layers.* Bachelor thesis (under preparation). TU Wien (2022).
36. D. Lundin et al. *High Power Impulse Magnetron Sputtering: Fundamentals, Technologies, Challenges and Applications.* Elsevier (2019).
37. D. Nečas et al. Gwyddion: an open-source software for SPM data analysis. *Open Physics* **10,** 181–188 (2012).
38. H. Urano. Roles of argon seeding in energy confinement and pedestal structure in JT-60U. *Nuclear Fusion* **55,** 033010 (2015).
39. J. Tirira et al. Elastic recoil detection analysis: Theoretical analysis of scattering cross section and basic parameters. *Journal of radioanalytical and nuclear chemistry* **130,** 311–319 (1989).
40. M. V. Moro et al. Accurate high-resolution depth profiling of magnetron sputtered transition metal alloy films containing light species: A multi-method approach. *Thin Solid Films* **686,** 137416 (2019).
41. B. M. Berger et al. Erosion of Fe-W model system under normal and oblige D ion irradiation. *Nuclear Materials and Energy* **12,** 468–471 (2017).
42. D. Onderdelinden. The influence of channeling on Cu single-crystal sputtering. *Applied Physics Letters* **8,** 189–190 (1966).
43. L. Spieß et al. *Moderne Röntgenbeugung.* Springer. (2009).

Die approbierte gedruckte Originalversion dieser Diplomarbeit ist an der TU Wien Bibliothek verfügbar
The approved original version of this thesis is available in print at TU Wien Bibliothek.

Acknowledgements

Im Zuge des Schreibens dieser Zeilen möchte ich die Gelegenheit ergreifen mich bei all jenen zu bedanken die mich bei der Durchführung dieser Arbeit aber auch auf meinem gesamten Weg durch dieses Studium stetig unterstützt und ermutigt haben.

Zunächst möchte ich mich besonders bei meinen Eltern Maria und Paul sowie meiner Schwester Stefanie bedanken. Es gibt mir besonderen Rückhalt zu wissen, dass ich stets auf eure Unterstützung bauen kann und ihr immer ein offenes Ohr für mich habt. Ebenso möchte ich der gesamten Arbeitsgruppe, allen voran Fritz, danken. Du stehst deinen Schützlingen bei Problemen immer zur Seite und bist stets bemüht deine Studierenden zu fördern sowie zu fordern. Du bewirkst ein durchwegs angenehm freundschaftliches Klima in deiner Arbeitsgruppe, und das schätze ich sehr. Nicht weniger möchte ich mich bei meinem Betreuer und Laborgefährten Christian bedanken. Du bist mir bei jeglichen experimentellen Schwierigkeiten stets mit Rat und Tat zur Seite gestanden und ich hoffe, dass du auch mögliche zukünftige kleine Laborstreiche weiterhin mit einem Schmunzeln entgegennimmst. Zudem wären die Stunden, die ich abseits des Labors im Büro verbracht habe, ohne die Mitglieder des Fusionsbüros kaum so amüsant gewesen, weshalb ich mich besonders bei Johannes, Lidija, Georg und Redl für die spaßigen Auflockerungen bedanken möchte. Auch diverse Kaffeepausen mit Kollegen haben mir den Arbeitsalltag erleichtert. An dieser Stelle möchte ich daher auch herzlichst Anna, Herbert, Gabriel, David, Matthias, Richard, Paul, Helmut und Daniel für die erbaulichen Erörterungen danken.
Furthermore, besides the valued colleagues at TU WIEN, I additionally want to seize the opportunity to thank our collaboration partners at Uppsala University, Daniel, Eduardo and Marcos, for your help analysing our samples and contributing to an enjoyable stay in the wonderful city of Uppsala.
Ein spezieller Dank gebührt auch der IAP Werkstatt mit Rainer Gärtner und Herbert Schmidt, die mir auch bei kniffligen Bauteilen im Zuge dieser Arbeit stets weitergeholfen haben. Für die Unterstützung bei weiterführenden Probenanalysen möchte ich an dieser Stelle außerdem auch Klaudia Hradil herzlich danken. Zu guter Letzt möchte ich mich ebenso bei meinen weiteren Lerngruppenmitgliedern bedanken, die sich mit mir gemeinsam durch so manche Prüfung gekämpft haben, sowie all meinen Freunden, die stets darum bemüht waren, mich auch in stressigen Studiensituationen vom Alltagstrott abzulenken.

Es war eine schöne Zeit, die durch eure Unterstützung möglich gemacht wurde, und dafür möchte ich euch allen herzlich danken.

Die approbierte gedruckte Originalversion dieser Diplomarbeit ist an der TU Wien Bibliothek verfügbar
The approved original version of this thesis is available in print at TU Wien Bibliothek.
TU Bibliothek Your knowledge hub WIEN

A. Beam shaping parameters

The following tables show the parameter values chosen for the irradiation experiments performed at the utilised sputtering setup at the Augustin laboratory at IAP TU Wien.

2keV Ar^+	
charge state	+1
ion species	argon
SPECS ion source parameters	
acceleration voltage	2000eV
extractor	93.98%
focus 1	97.98%
focus 2	0.00%
pos x	0.91mm
pos y	-2.14mm
width x	5mm
width y	varying: 0-5mm
L value	varying: 81mm or 88mm
emission current	10mA
WIEN filter parameters	
x_1	334.5V
x_2	405.6V
deflection	110.0V
working gas pressure parameters	
pressure value	$9.6 \cdot 10^{-5}$mbar

2keV D_2^+	
charge state	+1
ion species	deuterium
SPECS ion source parameters	
acceleration voltage	2000eV
extractor	94.94%
focus 1	80.26%
focus 2	0.00%
pos x	-0.84mm
pos y	-0.76mm
width x	5mm
width y	varying: 2.5-5mm
L value	varying: 81mm
emission current	10mA
WIEN filter parameters	
x_1	363.4V
x_2	403.4V
deflection	311.5V
working gas pressure parameters	
pressure value	$1.5 \cdot 10^{-4}$mbar

Figure A.1.: Listing of the utilised values for the beam shaping components in the experimental setup. In addition, a Wien-filter permanent magnet, mounted to the outside of the beam shaping section of the apparatus, was used.

It should be mentioned that the collapsed value of 0 mm for the beam scanning width in y direction was used only during the catcher cleaning process in the catcher profile measurement routine (compare step 3 in chapter 3.2.3). Additionally, the L value of 88 mm was used only during the *in-situ* layer creation (compare chapter 3.3).

Die approbierte gedruckte Originalversion dieser Diplomarbeit ist an der TU Wien Bibliothek verfügbar
The approved original version of this thesis is available in print at TU Wien Bibliothek.
TU Bibliothek Your knowledge hub WIEN

B. Constructional elements for the manipulator motorisation

The following sketches are meant to function as an overview of the constructional elements needed for the manipulator motorisation, achieved in the course of this thesis. More detailed drawings also containing technical dimensions can be provided upon request.

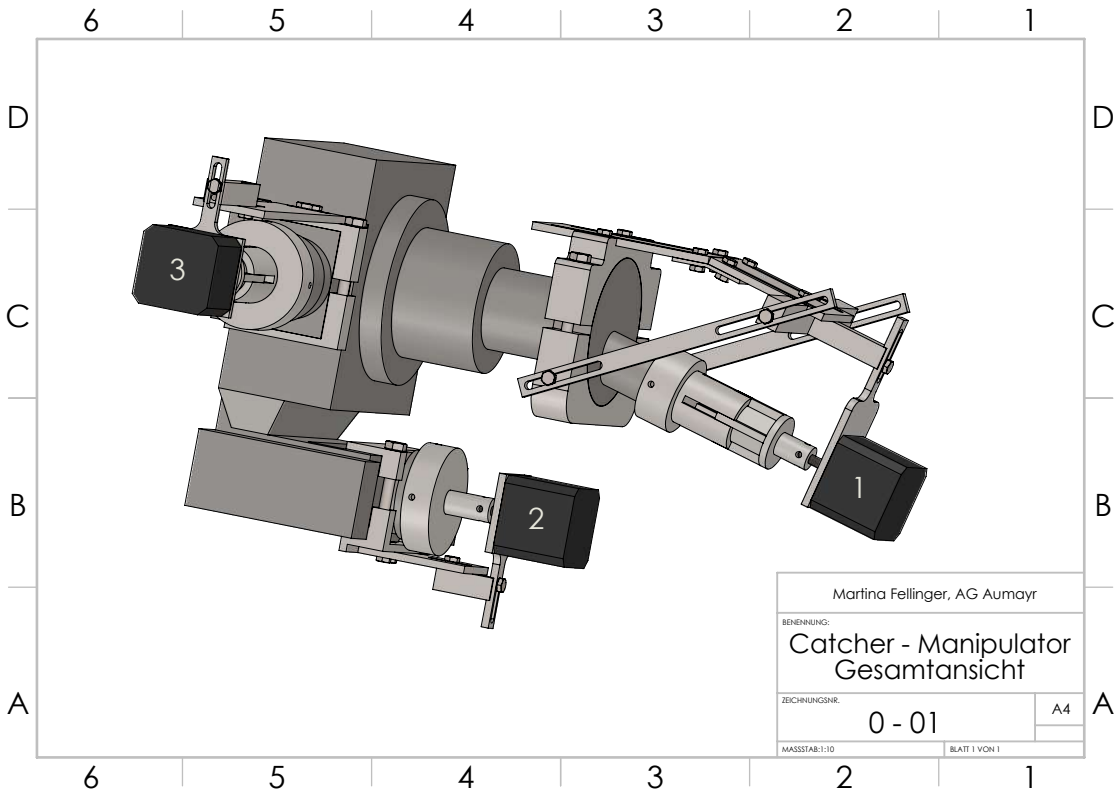

Die approbierte gedruckte Originalversion dieser Diplomarbeit ist an der TU Wien Bibliothek verfügbar
The approved original version of this thesis is available in print at TU Wien Bibliothek.
TU Bibliothek Your knowledge hub WIEN

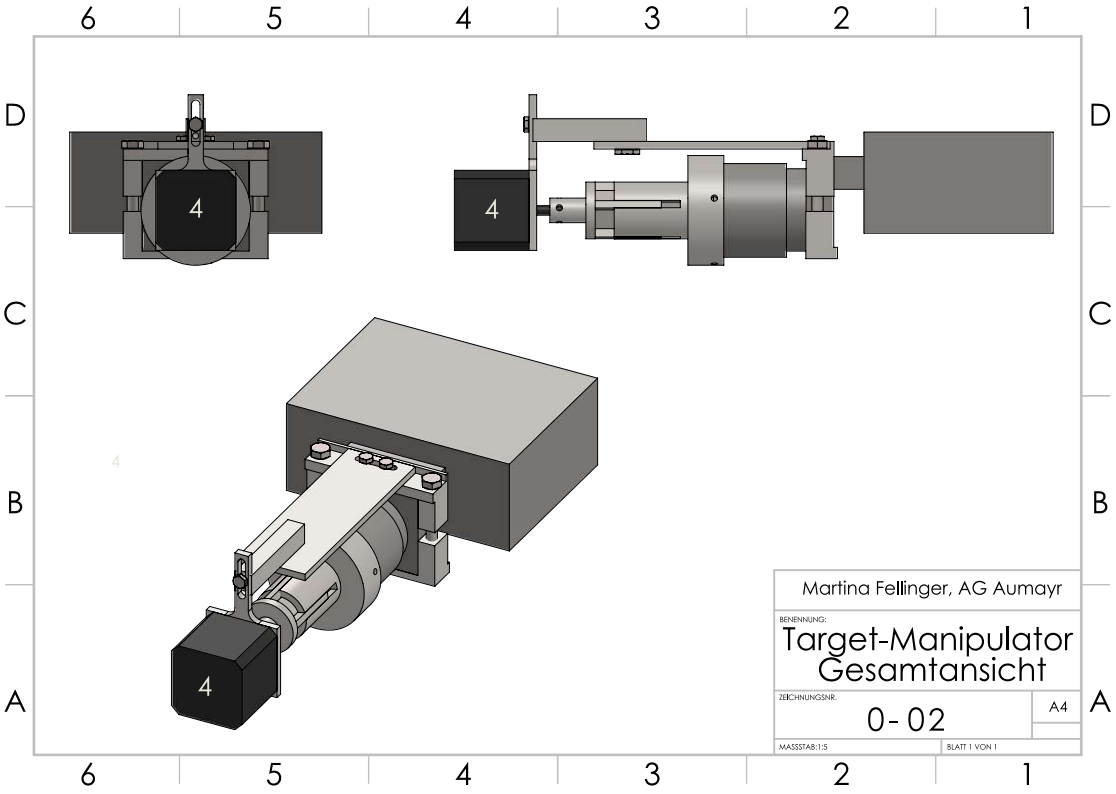

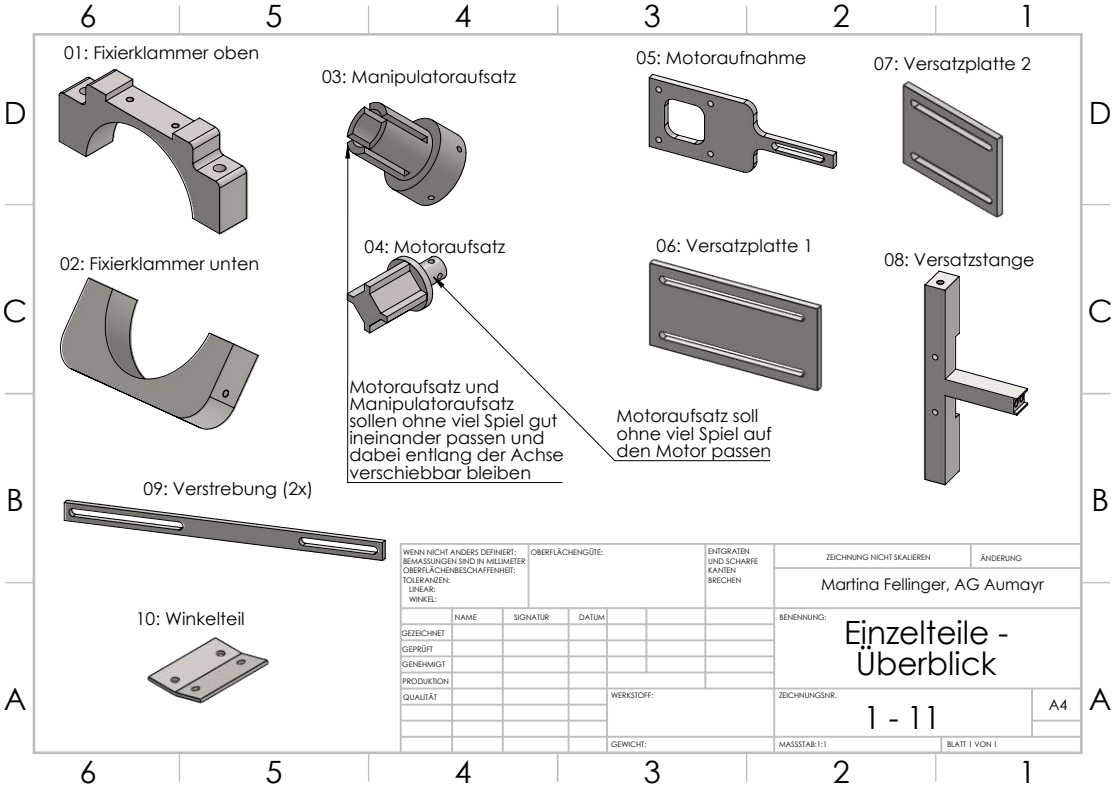

Die approbierte gedruckte Originalversion dieser Diplomarbeit ist an der TU Wien Bibliothek verfügbar
The approved original version of this thesis is available in print at TU Wien Bibliothek.

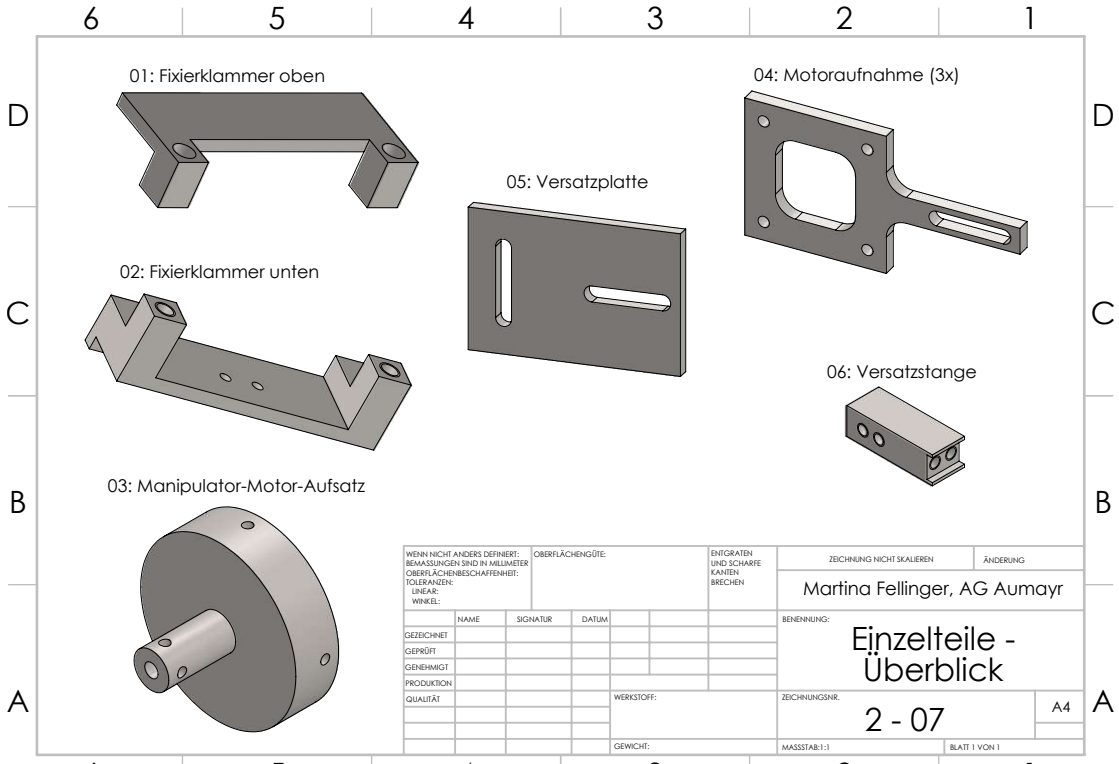

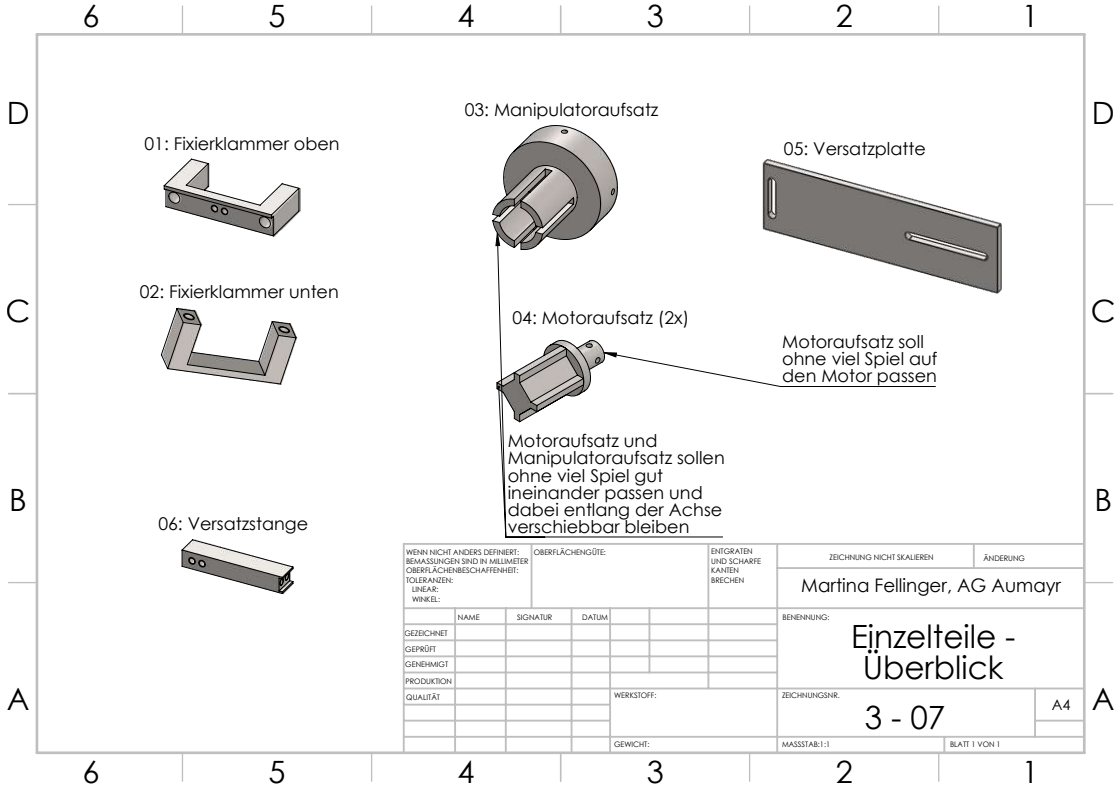

Die approbierte gedruckte Originalversion dieser Diplomarbeit ist an der TU Wien Bibliothek verfügbar
The approved original version of this thesis is available in print at TU Wien Bibliothek.

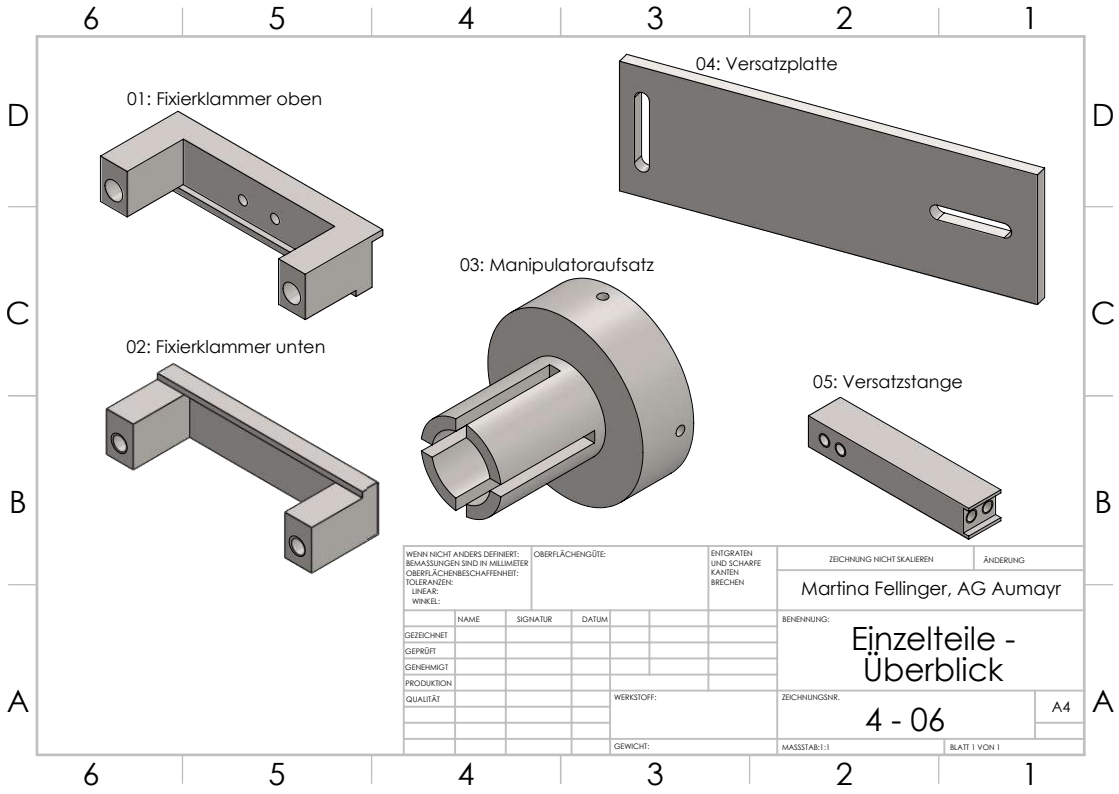

Die approbierte gedruckte Originalversion dieser Diplomarbeit ist an der TU Wien Bibliothek verfügbar
The approved original version of this thesis is available in print at TU Wien Bibliothek.

C. Catcher positioning table

The subsequent table shows the precise manipulator positions that were used in order to drive a circular catcher profile around the target at a radial distance of 21.4 mm. A y-tilt$_{catcher}$ value of 9.00 is set to correspond to parallel alignment with the beam direction.

tilt angle	y-tilt$_{catcher}$	x$_{catcher}$	y$_{catcher}$	z$_{catcher}$ (fixed)
-25	13,22	-4,04	56,89	1,2 (black)
-20	12,45	-2,32	57,61	1,2 (black)
-15	11,63	-0,54	58,17	1,2 (black)
-7,5	10,36	2,21	58,72	1,2 (black)
-5	9,91	3,13	58,82	1,2 (black)
0	9,00	5,00	58,90	1,2 (black)
5	8,08	6,87	58,82	1,2 (black)
10	7,14	8,72	58,57	1,2 (black)
15	6,20	10,54	58,17	1,2 (black)
20	5,27	12,32	57,61	1,2 (black)
25	4,35	14,04	56,89	1,2 (black)
30	3,45	15,70	56,03	1,2 (black)
35	2,58	17,27	55,03	1,2 (black)
40	1,76	18,76	53,89	1,2 (black)
45	0,98	20,13	52,63	1,2 (black)
50	0,26	21,39	51,26	1,2 (black)
55	-0,39	22,53	49,77	1,2 (black)
60	-0,98	23,53	48,20	1,2 (black)
65	-1,49	24,39	46,54	1,2 (black)
70	-1,91	25,11	44,82	1,2 (black)
75	-2,24	25,67	43,04	1,2 (black)
80	-2,49	26,07	41,22	1,2 (black)

Declaration:

x$_{catcher}$: position of quartz along ion beam direction (see axis 3 in figures 3.2 - 3.4 in chapter 3.2)

y$_{catcher}$: position of quartz perpendicular to ion beam direction (see axis 2 in figures 3.2 - 3.4 in chapter 3.2)

z$_{catcher}$: position vertically, here always in center x-y plane of laboratory axis

y-tilt$_{catcher}$: linear movement for tilting the catcher quartz (see axis 1 in figures 3.2 - 3.4 in chapter 3.2)

Figure C.1.: Manipulator positions for a circular catcher profile, table adapted from [25].

Die approbierte gedruckte Originalversion dieser Diplomarbeit ist an der TU Wien Bibliothek verfügbar
The approved original version of this thesis is available in print at TU Wien Bibliothek.